



# **JGR** Oceans

## **RESEARCH ARTICLE**

10.1029/2023JC020761

### **Key Points:**

- Global altimetry-based products evaluated to study Gulf Stream rings differ from regional data products based on sea surface temperature
- Global products do not detect an observed regime shift in the number of Warm Core Ring formations and do not reflect the known seasonality
- A shift to a higher energy state in the Northwest Atlantic around 2000 is detected via satellite altimetry-based geostrophic velocities

#### Correspondence to:

E. Perez, eperez@whoi.edu

#### Citation:

Perez, E., Andres, M., & Gawarkiewicz, G. (2024). Is the regime shift in Gulf Stream warm core rings detected by satellite altimetry? An inter-comparison of eddy identification and tracking products. *Journal of Geophysical Research: Oceans*, 129, e2023JC020761. https://doi.org/10.1029/2023JC020761

Received 28 NOV 2023 Accepted 9 SEP 2024

#### **Author Contributions:**

Conceptualization: M. Andres,
G. Gawarkiewicz
Data curation: E. Perez
Formal analysis: E. Perez
Funding acquisition: M. Andres
Investigation: E. Perez
Methodology: E. Perez
Project administration: M. Andres,
G. Gawarkiewicz
Supervision: M. Andres,
G. Gawarkiewicz
Visualization: E. Perez
Writing – original draft: E. Perez
Writing – review & editing: E. Perez,
M. Andres, G. Gawarkiewicz

© 2024. The Author(s).

This is an open access article under the terms of the Creative Commons

Attribution-NonCommercial-NoDerivs

License, which permits use and distribution in any medium, provided the original work is properly cited, the use is non-commercial and no modifications or adaptations are made.

# Is the Regime Shift in Gulf Stream Warm Core Rings Detected by Satellite Altimetry? An Inter-Comparison of Eddy Identification and Tracking Products

E. Perez<sup>1,2</sup>, M. Andres<sup>2</sup>, and G. Gawarkiewicz<sup>2</sup>

<sup>1</sup>MIT-WHOI Joint Program in Oceanography/Applied Ocean Sciences & Engineering, Woods Hole, MA, USA, <sup>2</sup>Woods Hole Oceanographic Institution, Woods Hole, MA, USA

**Abstract** Downstream of Cape Hatteras, the vigorously meandering Gulf Stream forms anticyclonic warm core rings (WCRs) that carry warm Gulf Stream and Sargasso Sea waters into the cooler, fresher Slope Sea, and forms cyclonic cold core rings (CCRs) that carry Slope Sea waters into the Sargasso Sea. The Northwest Atlantic shelf and open ocean off the U.S. East Coast have experienced dramatic changes in ocean circulation and water properties in recent years, with significant consequences for marine ecosystems and coastal communities. Some of these changes may be related to a reported regime shift in the number of WCRs formed annually, with a doubling of WCRs shed after 2000. Since the regime shift was detected using a regional eddytracking product, primarily based on sea surface temperatures and relies on analyst skill, we examine three global eddy-tracking products as an automated and potentially more objective way to detect changes in Gulf Stream rings. Currently, global products rely on altimeter-measured sea surface height (SSH), with WCRs registering as sea surface highs and CCRs as lows. To identify eddies, these products use either SSH contours or a Lagrangian approach, with particles seeded in satellite-based surface geostrophic velocity fields. This study confirms the three global products are not well suited for statistical analysis of Gulf Stream rings and suggests that automated WCR identification and tracking comes at the price of accurate identification and tracking. Furthermore, a shift to a higher energy state is detected in the Northwest Atlantic, which coincides with the regime shift in WCRs.

Plain Language Summary In the Northwest Atlantic Ocean, a specific type of eddy, known as a ring, is formed by the Gulf Stream, a strong ocean current that closely follows the U.S. East Coast between Florida and Cape Hatteras. Northeast of Cape Hatteras, the Gulf Stream separates from the continental shelf and starts to meander. Sometimes, these meanders grow into oxbow-like structures that pinch off from the Gulf Stream and become rings. Warm core rings (WCRs) are formed north of the Gulf Stream, with warm centers that create sea surface hills. In contrast, cold core rings (CCRs) form south of the stream, with cold centers and sea surface valleys. Since 1980 an analyst, who studies the Gulf Stream, has used primarily sea surface temperature to identify WCRs. A regional Ring Census based on this work found a doubling in WCR formations after 2000. Other eddy data sets are based on satellite data, such as sea surface height (SSH), and are created by automated tracking algorithms. This study compares global eddy data sets with the Ring Census. Our findings suggest global data sets using SSH alone cannot replicate the results of the Ring Census. Additionally, we find the Northwest Atlantic region has become more energetic since 2000.

#### 1. Introduction

Warm and cold core rings (WCRs and CCRs) are types of mesoscale eddies that are formed by the Gulf Stream. These rings can transport water masses across the Gulf Stream front and westward hundreds of kilometers from their formation site until they dissipate or are reabsorbed by the Gulf Stream. WCRs are well-studied on account of their importance for heat and salt transport and their interactions with other regional flows (Flierl, 1979; Silver et al., 2021). WCRs in the Northwest Atlantic impact the regional physical (Zhang & Gawarkiewicz, 2015), biological (Braun et al., 2019), and chemical oceanography (Conway et al., 2018). Gulf Stream rings typically have a diameter on the order of 100 km, can exist as a coherent feature for a few days to a few hundred days, and have a vertical scale that can extend from the surface to depths of 500–1,000 m (Csanady, 1979; Flierl, 1979; Gangopadhyay et al., 2020; Joyce, 1984, 1991).

PEREZ ET AL. 1 of 22

The Gulf Stream separates from the continental slope east of Cape Hatteras, North Carolina, and follows a time-varying, meandering path. Here, the Gulf Stream is a front between the cold, fresh Slope Sea and the warm, salty Sargasso Sea. Sometimes, a meander crest (trough) will become so large that it contorts on itself and "pinches off" to form an anticyclonic (cyclonic) ring (Fuglister, 1972). A WCR can also be formed via a different mechanism to generate an "aneurysm," which occurs when the cyclonic flank of the Stream bulges into the Slope Sea and then a ring detaches from the main current (A. R. Richardson, 1983; P. L. Richardson et al., 1978; Silver et al., 2022). Aneurysm (or aneurism, as written by A. R. Richardson (1983)) rings tend to be smaller with radii of ~50 km, have shallower thermoclines, and have cores of Gulf Stream water rather than Sargasso Sea water (A. R. Richardson, 1983; Silver et al., 2022), but similar to pinch-off WCRs, they are also anticyclones and are also warmer than the ambient Slope Sea water.

As Gulf Stream rings translate through the Slope Sea, they carry the characteristics of the water mass of their formation location in their SST and sea surface height (SSH) signatures. Pinch-off WCRs are sea surface highs with a core of Sargasso Sea water surrounded by a perimeter of Gulf Stream water; aneurysm WCRs have only Gulf Stream water. Both types of WCRs translate west or southwestward after they are formed. CCRs are sea surface lows with a core of Slope Sea water and also translate southwestward.

The following analysis distinguishes between a Gulf Stream ring, which is a feature shed from the Gulf Stream, and the more general eddy. An eddy can be any coherent, rotating structure of water, irrespective of its formation mechanism. Mesoscale eddies typically range in diameter from 10 to 500 km and can persist for a few days to a few hundred days. In this context, a ring is a specific type of eddy formed from a western boundary current—in this case, the Gulf Stream—and is associated with an isolated mass of water that varies significantly from the ambient water surrounding the ring (Csanady, 1979). Analogous rings are also shed from the Agulhas Current and propagate across the South Atlantic, carrying warm, salty water from the Indian Ocean subtropical gyre into the South Atlantic (Lutjeharms, 1981). Eddies are shed from the Loop Current and move westward through the Gulf of Mexico (e.g., Hamilton et al., 1999). Gulf Stream rings are mesoscale eddies, but not all mesoscale eddies in the Northwest Atlantic are Gulf Stream rings.

A non-linear eddy can trap fluid in its center and transport heat, salt, and potential vorticity as it translates (Flierl, 1979); this is in contrast to a linear wave in which an SSH signature can translate through the background temperature and salinity field without advecting the water masses. Although the notion that a ring is a non-linear eddy formed from the Gulf Stream that carries distinct water mass characteristics is well established, how to identify an eddy in observations is ambiguous. The difficulty in eddy identification lies in the struggle to separate a coherent eddy from other types of time-dependent oceanic motions ("eddying motions"), especially in regions of high mesoscale variability that can have elevated eddy kinetic energy (EKE) even when there is no coherent eddy present, as can be the case in the meandering Gulf Stream. Past eddy studies have employed the Okubo-Weiss parameter (sum of strain minus relative vorticity), differences in SSH, rotational speed, potential vorticity, velocity streamlines, Lyapunov exponents, and Lagrangian-averaged vorticity deviation to identify eddies (Abernathy & Haller, 2018; Chelton et al., 2007, 2011; Faghmous et al., 2015; Haller et al., 2016; Isern-Fontanet et al., 2003, 2004; Kurian et al., 2011; Morrow et al., 2004; Nencioli et al., 2010; Shadden et al., 2005). These various methods of eddy identification are either Eulerian or Lagrangian; both methods have advantages and disadvantages.

The Northwest Atlantic has experienced many changes in recent decades. Andres (2016) found that the longitude where Gulf Stream meanders reach large amplitude, that is, the "destabilization point," undergoes substantial interannual variability and has shifted westward relative to the location of the destabilization point in 1995. Observations collected from 2014 to 2016 recorded anomalous shelf and slope conditions south of New England, indicative of more frequent onshore intrusions of warm, salty waters in recent years (Gawarkiewicz et al., 2018). Holliday et al. (2020) found that the Northwest Atlantic underwent a marked salinification in concert with an extreme freshening in the sub-polar North Atlantic from 2012 to 2016 (see their Figure 6). Gonçalves Neto et al. (2021) showed that the Gulf Stream position migrated closer to the Tail of the Grand Banks in 2008, a change that has persisted since and preceded subsequent warming of the Northwest Atlantic Shelf, likely by reducing connectivity between the cool Labrador Current and the shelf waters west of the Grand Banks. Pershing et al. (2015) found that from 2005 to 2015, the Gulf of Maine warmed faster than 99% of the world's oceans. Additionally, Forsyth et al. (2015) found that the recent warming on the continental shelf and upper slope is not confined to the sea surface but extends into the subsurface ocean.

PEREZ ET AL. 2 of 22

Some of these changes in the Northwest Atlantic may be related to Gulf Stream rings. Gangopadhyay et al. (2019) identified a regime shift in Gulf Stream WCRs, with annual formation rates after 2000 nearly double those before 2000. Silver et al. (2021) expanded on this work to include CCRs and did not detect a corresponding regime shift for CCRs. The doubling of WCRs produced annually after the regime shift has implications for the ecosystems of the Northeast shelf and slope, as well as the dynamics and circulation of this region (Gawarkiewicz et al., 2022; Silver et al., 2023). Silver et al. (2021) also reported that the doubling in WCRs has increased net northward heat transport into the Slope Sea north of the Gulf Stream. Gangopadhyay et al. (2019) and Silver et al. (2021) found that most WCRs and CCRs are formed between 65°W and 60°W (which they identify as Zone 3), and the fewest are formed between 75°W and 70°W (their Zone 1). The authors found that CCR formations peak in May, while WCR formations peak in July.

In light of the difficulty in eddy-detection, and motivated by the reported WCR regime shift detected in SST-based ring products (Gangopadhyay et al., 2019; Silver et al., 2021), we investigate whether satellite altimetry-based products can capture the same results. Four products are evaluated in this study. The baseline for our comparison is the regional product, the Ring Census, that Gangopadhyay et al. (2019) and Silver et al. (2021) used to identify the WCR regime shift. The other three are global products based on automated detection schemes for eddy identification using mapped satellite altimetry. Here, we compare the global eddy products to the Ring Census and use the Ring Census as the standard for comparison both because it is the longest record of Gulf Stream WCRs, and because it has been extensively validated by numerous regional studies of WCRs and their impacts.

The paper is organized as follows. Section 2 presents the eddy data products and auxiliary data sets used here for interpretation. Section 3 describes the methods used to subset global eddy products to isolate Gulf Stream rings from other types of eddies identified in the global products. Section 4 reports the results of the data product intercomparison and an analysis of the energetics of the Northwest Atlantic, and Section 5 discusses the results. Finally, Section 6 concludes with some thoughts on the limitations of the global SSH-based products and the change in the energetics of the Northwest Atlantic.

#### 2. Data

Here, we use four products that identify and track eddies (Table 1). One is a regional product mainly based on SST, and the other three are global products that rely on satellite-measured SSH to identify mesoscale eddies. Gangopadhyay et al. (2020) created the Ring Census (Gangopadhyay & Gawarkiewicz, 2020) using the Northwest Atlantic composite charts produced by Jenifer Clark, hereafter referred to as the analyst, called "Clark charts," to identify and track Gulf Stream WCRs. Two versions of the global Mesoscale Eddy Trajectories Atlas (META) are considered here: META2.0 and META3.1exp. META2.0 is the first global product in which an algorithm automatically detects mesoscale eddies, initially presented by Chelton et al. (2011) and updated by Schlax and Chelton (2016), and uses closed contours of SSH anomalies to identify eddies. META3.1exp is an update to META2.0 developed by Pegliasco et al. (2022) and relies on total SSH (absolute dynamic topography) rather than SSH anomaly. GLED v1.0 uses a Lagrangian mesoscale eddy algorithm that considers particle trajectories as an alternative to the contour-based eddy-identification schemes used in products such as META2.0 and META3.1exp (Liu & Abernathey, 2022). The particle trajectories for GLED v1.0 are calculated from SSH-based surface geostrophic velocities. Sections 4 and 5 primarily discuss comparisons between the Ring Census and META2.0. However, the newer products, META3.1exp and GLED v1.0, are also examined briefly.

### 2.1. The Ring Census From Clark Charts

The Clark charts are annotated SST maps of the Northwest Atlantic that have been consistently produced two or three times per week since 1980 by an analyst who blends satellite infra-red imagery and in situ surface temperature observations to create high horizontal resolution (1.1 km), 3-day composite SST images. Although the Clark charts are primarily based on SST, the analyst sometimes uses SSH from satellite altimetry to help interpret features not evident in the SST images (Silver et al., 2021), which can sometimes have gaps due to cloud cover. Several previous studies used the Bedford Institute of Oceanography data to validate the charts and assess analyst error (Monim, 2017; Silva, 2019). Oceanic circulation features, such as the Gulf Stream and its rings, are marked on the charts and thus can be tracked from one chart to the next. Using a Geographical Information System framework, Gangopadhyay et al. (2020) digitized the charts. They cataloged the date, location, and size of each

PEREZ ET AL. 3 of 22

Table 1
Summary of Data Products Used in This Paper

NEW CO.							
	Ring Census	META2.0	META3.1exp	GLED v1.0			
Min. lifespan	≥7 d	≥28 d	≥28 d	30 d, 90 d, and 180 d trajectories			
Size (radius, km)	$R \ge 20 \text{ km}$	$R \ge 40 \text{ km}$	$R \ge \sim 30 \text{ km}$	$R \ge 25 \text{ km}$			
	Preferred $R = 50-100 \text{ km}$	In NWA, $R_{avg.} \approx 70 \text{ km}$	In NWA, $R_{avg.} \approx 50 \text{ km}$	In NWA, $R_{avg.} \approx 45 \text{ km}$			
Period	1980–2017	1993-March 2020	1993-March 2020	1993–2019			
Methodology	An analyst creates charts of the region, which are then processed, validated, and turned into the Ring Census	The algorithms to identify and track eddies are derived from Chelton et al. (2011) and described in Schlax and Chelton (2016)	The algorithm to identify and track eddies is derived from Mason et al. (2014) and described in Pegliasco et al. (2022)	Lagrangian method by Haller et al. (2016) is used to identify rotationally coherent Lagrangian vortices			
Data set(s) used	Primarily SST for the charts, additionally in situ temperature data and SSH	SSH, specifically sea level anomalies	SSH, specifically absolute dynamic topography	Geostrophic velocity fields derived from sea level anomalies			
Coverage	Northwest Atlantic	Global	Global	Global			
	$(30^{\circ}N-45^{\circ}N, 75^{\circ}W-55^{\circ}W)$						
Eulerian or Lagrangian?	Eulerian	Eulerian	Eulerian	Lagrangian			
Notes	No longer recommended for use cf. Pegliasco et al. (2022)						

WCR noted on the charts from its birth to its demise to create the WCR Census (1980–2017) (see Gangopadhyay et al. (2019, 2020) for a description of this procedure). Silver et al. (2021) reprocessed the charts from 1980 through 2019 for WCRs. They employed a similar methodology to create a separate CCR Census (see the Data Availability Section of Silver et al. (2021)). These previous WCR studies separated the study region (30°N–45°N, 75°W–55°W) into four subregions (Zone 1: 75°W–70°W, Zone 2: 70°W–65°W, Zone 3: 65°W–60°W, and Zone 4: 60°W–55°W). These zones are adopted here to allow for a consistent comparison of the global data products with the chart-based Ring Census. WCRs identified by the Ring Census tend to have radii between 50 and 100 km; the smallest WCRs included in the Ring Census have radii of 20 km (Table 1). For an example of a Clark chart, see Figure 1a of Gangopadhyay et al. (2019) or Figure 1 of Silver et al. (2022).

#### 2.2. Altimeter-Based Ring Tracking

Satellite altimeters measure global ocean topography, a dynamic field that reflects large- and mesoscale oceanic processes, including mesoscale eddies. Mesoscale eddies have SSH signatures that correspond with their rotation —anticyclones have an SSH high at their center, and cyclones have an SSH low. By merging along-track observations from multiple satellites, the resolution of SSH fields is nominally high enough to resolve mesoscale eddies (Chelton et al., 2011).

## 2.2.1. META2.0

The META Product (META2.0) is a global database comprising mesoscale eddies identified and tracked from satellite altimetry using an algorithm developed by Chelton and Schlax (Chelton et al., 2011; Schlax & Chelton, 2016). Schlax and Chelton (2016) consider an eddy to be a compact and coherent propagating structure as identified in mapped SSH. META2.0 merges the SSH measurements from two simultaneously operating altimeters to create high-resolution SSH maps with about 40 km feature resolution. Due to the orbital periods of the altimeters (about 10-day repeat cycles for the Jason/Topex satellites and 35 days for the European Space Agency satellites), the mapped SSH fields have difficulty resolving features with lifetimes shorter than 4 weeks. Thus, META2.0 excludes eddies with lifetimes shorter than 4 weeks from the product. With this temporal and spatial resolution, META2.0 should, in principle, capture features that the Ring Census detects (Table 1). The META2.0 procedure applies the "growing method" to identify eddies in SSH fields: the algorithm discretizes the field into 2D pixels, locates a local maximum (SSH high) or minimum (SSH low) pixel, checks if the SSH values of

PEREZ ET AL. 4 of 22

neighboring pixels pass a certain threshold to create a set of pixels, and then if all pixels in the set satisfy five criteria, the set is considered to be an eddy. The five criteria are defined by Schlax and Chelton (2016) for compact and coherent structures.

#### 2.2.2. META3.1exp and GLED v1.0

Two recent studies have produced new eddy products. These are META3.1exp, a new, improved version of META2.0, and a global Lagrangian eddy data (GLED v1.0) product, which is a Lagrangian alternative to the META products that are based on SSH contours. These new products are not the focus of this study (primarily a comparison of the Ring Census and META2.0), but they are considered for completeness and are described below.

Pegliasco et al. (2022) introduced META3.1exp, a new global atlas of mesoscale eddies based on SSH. MET-A3.1exp uses an eddy-tracker algorithm developed by Mason et al. (2014). It improves upon META2.0 by using absolute dynamic topography (i.e., SSH) instead of sea level anomaly (i.e., SSHa) to better resolve closed circulation features in energetic regions. Therefore, META3.1exp is expected to perform better than META2.0, particularly in regions with a meandering current, such as the Gulf Stream.

Liu and Abernathey (2023) developed GLED v1.0, the Lagrangian alternative to eddy products such as MET-A3.1exp. Liu and Abernathey (2023) use satellite-derived surface geostrophic velocities to define a velocity field and then seed this field with Lagrangian particles. The Lagrangian particles are advected with satellite-derived surface geostrophic velocities. Using the method of Lagrangian-averaged vorticity deviation, they can identify and track eddies with lifetimes of 30, 90, and 180 days. Interestingly, these Lagrangian-defined eddies tend to be smaller than the SSH contour-based eddies.

#### 2.2.3. Other Data Sets

To help cross-compare the four data products, we apply some filtering and subsetting described in Section 3. One step in this process relies on identifying the (daily) location of the Gulf Stream. Here, the Gulf Stream daily paths are identified using the 25 cm SSH contour in daily mapped SSH fields (1993–2022) after Andres (2016) since this contour serves as a good proxy for the Gulf Stream axis (see Andres et al. (2020), their Figure 3). Gridded bathymetry data from the General Bathymetric Chart of the Oceans (spanning 24°N–53°N, 82°W–48°W) is also used for the filtering procedure (to identify the shelf, where WCRs, which are deep-reaching features, cannot exist, but where other eddy types might exist as coherent rotating features).

We use several auxiliary data sets to compare individual features identified in the various products (Section 5). This includes SST from NOAA's 1/4° Daily Optimum Interpolation sea surface temperature product (Huang et al., 2020) and daily SSH maps from Copernicus Marine Environment Monitoring Survey's Global Ocean Gridded SSH product. See the Data Availability Section for information on accessing these data sets.

## 3. Methods

## 3.1. Subsetting and Filtering

To better compare the global eddy products to the regional Ring Census, we first subset the WCRs from the Ring Census to match the temporal and spatial resolution of features expected to be identified by META2.0. That is, we subset the Ring Census to include only rings for the overlapping period (1993–2017) that (a) live long enough to be identified and tracked by the META2.0 algorithm ( $\geq 4$  weeks) and (b) are large enough to be identified and tracked by META2.0 (radius  $\geq 40$  km).

The global eddy products (META2.0, META3.1exp, and GLED v1.0) are not designed to differentiate Gulf Stream rings from all other coherent eddy features. Therefore, to compare the META2.0 data product (or other global products) to the Ring Census, it is necessary to filter the META2.0 eddies to isolate those eddies that could have formed from the Gulf Stream and could, therefore, be considered rings (Figure 1). The full (unfiltered) META2.0 eddy data product for the 1993–2017 period identifies 3,371 eddies in the latitude and longitude box (30°N–45°N, 75°W–55°W), which is the region examined in the Ring Census (Gangopadhyay et al., 2019): 1,801 anticyclones and 1,570 cyclones. The trajectories are shown in Figure 1a. The Ring Census identifies only 729

PEREZ ET AL. 5 of 22

21699291, 2024, 10, Downloaded from https://agupubs.onlinelibrary.wiley.com/doi/10.1029/2023JC020761 by Mbl Whoi Library, Wiley Online Library on [08/10/2024]. See

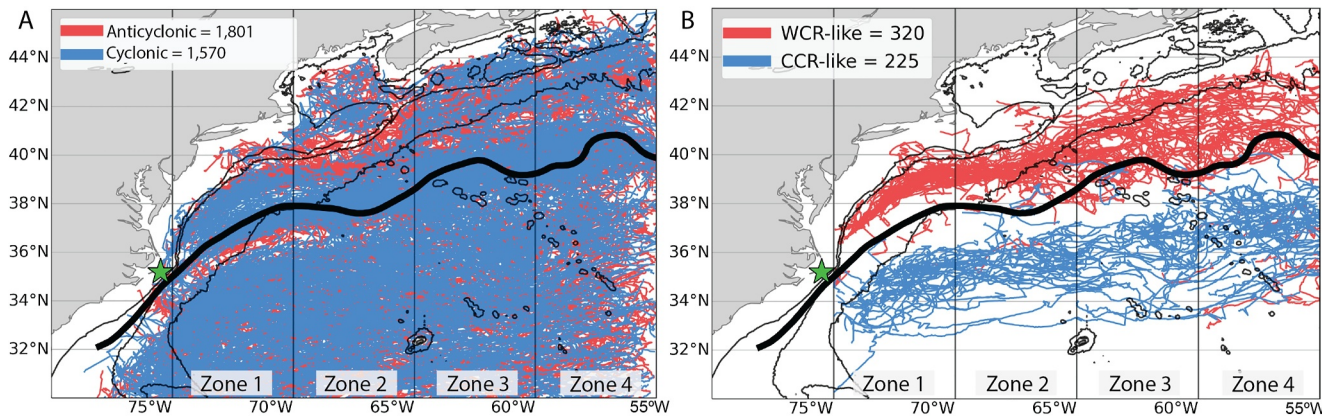


Figure 1. (a) Map of the Northwest Atlantic region (30°N-45°N, 75°W-55°W) considered in this study that shows eddy trajectories for anticyclones (red) and cyclones (blue) from the META2.0 product before filtering, with 1,801 anticyclones and 1,570 cyclones. (b) As in (a), but after filtering (described in Section 3) with 320 warm core ring-like eddies and 225 cold core ring-like eddies. The thin black dashed lines show isobaths at 100, 1,000, and 4,000-m depth. The thick black line is the mean Gulf Stream path averaged over 1993–2022 plotted for reference. The four thin black vertical lines signify the zones Gangopadhyay et al. (2019) and Silver et al. (2021) used; Zone 1:  $75^{\circ}W - 70^{\circ}W$ , Zone 2:  $70^{\circ}W - 65^{\circ}W$ , Zone 3:  $65^{\circ}W - 60^{\circ}W$ , and Zone 4:  $60^{\circ}W - 55^{\circ}W$ . The green star is the location of Cape Hatteras, approximately where the Gulf Stream separates from the continental shelf.

WCRs for the same region and period. The CCR Census has not been published, see Silver et al. (2021) for more details on data accessibility.

Most eddies identified in META2.0 are not features generated from the Gulf Stream and, therefore, do not represent WCRs or CCRs. So, we filter META2.0 global eddy products (and the other global eddy products) based on their formation location relative to the meandering Gulf Stream to derive a product that contains only "WCR-like" and "CCR-like" eddies. We make the distinction here between WCR and WCR-like because, without SST or subsurface data within a given feature, it is not possible to conclude with certainty that an eddy identified by META2.0 (or META3.1exp or GLED v1.0) based on SSH is, in fact, a closed circulation with an isolated fluid core.

To classify an eddy identified in a global product as WCR-like, it must be (a) anticyclonic, (b) westward propagating, (c) formed within an envelope that is between 3°N and 0.25°S of the Gulf Stream daily path, and (d) not formed on the continental shelf (shoreward of the 100 m isobath). To classify an eddy as CCR-like, it must be (a) cyclonic, (b) westward propagating, (c) formed within an envelope that is between 3°S and 0.25°N of the Gulf Stream daily path, (d) not formed on the continental shelf (shoreward of the 100 m isobath), and (e) formed north of 34°N which is approximately the latitude at which the Gulf Stream separates from the continental shelf east of Cape Hatteras.

In the case of WCR-like eddies, we allow 0.25° to the south of the Gulf Stream path in the envelope because of some uncertainty in the identification of the Gulf Stream path from satellite altimetry, due to the coarse spatial resolution. To define the northern edge of the envelope, we choose a 3° boundary northward of the Gulf Stream daily path. These envelope boundaries are chosen to allow for uncertainty in the exact location of the GS and to account for the typical diameters of large Gulf Stream pinch off rings which can range from 100 to 300 km. We choose a 3° boundary northward of the time-varying Gulf Stream daily path. Results are somewhat sensitive to the location of this northern boundary. Ultimately these envelope boundaries are chosen to allow for uncertainty in the exact location of the GS and to account for the typical diameters of large Gulf Stream pinch off rings which can range from 100 to 300 km. The filter method can be accessed in the GitHub repository for this project (see Data Availability Section).

Notably, after the META2.0 eddies are filtered to include only ring-like eddies (Figure 1b), the number of WCRlike eddies (320) is less than the number of WCRs recorded by the Ring Census (406). Similar filtering procedures are used for the other global products (META3.1exp and GLED v1.0).

Since META2.0 is the oldest and most widely used global product, the comparison of satellite products is mainly between the Ring Census and META2.0. Henceforth, "subset WCRs" will refer to the WCRs from the Ring

PEREZ ET AL. 6 of 22 175 150

125

75 50 25

200

175 150

C

CCR-like

WCR-like

Zone 1

Zone 2

Number of Formations

WCR

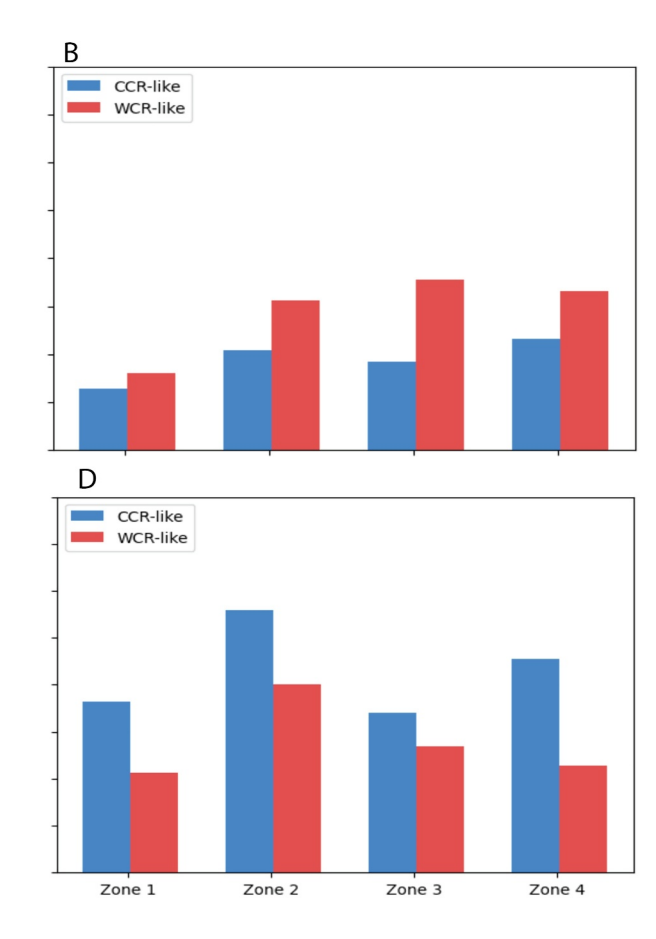


Figure 2. Distribution of formations per zone (Zone 1:  $75^{\circ}\text{W}-70^{\circ}\text{W}$ , Zone 2:  $70^{\circ}\text{W}-65^{\circ}\text{W}$ , Zone 3:  $65^{\circ}\text{W}-60^{\circ}\text{W}$ , and Zone 4:  $60^{\circ}\text{W}-55^{\circ}\text{W}$ ) for (a) the Ring Census warm core rings (WCRs) (red) subset by resolution and period of META2.0 ( $R \ge 40 \text{ km}$ , lifespan  $\ge 4 \text{ weeks}$ ), (b) META2.0 WCR-like eddies (red) and cold core ring (CCR)-like eddies (blue), (c) META3.1exp WCR-like eddies (red) and CCR-like eddies (blue), and (d) GLED v1.0 WCR-like eddies (red) and CCR-like eddies (blue).

Zone 4

Census subset by resolution and period of META2.0 (1993–2017,  $R \ge 40$  km, lifespan  $\ge 4$  weeks), and "WCR-like eddies" will refer to the filtered, anticyclonic META2.0 eddies, unless otherwise noted. Comparisons with the newer products, META3.1exp and GLED v1.0, are included at the end of Section 4, Results, and Section 5, Discussion. The following section also includes results for the CCR-like eddies (from the filtered global products) for completeness, but does not discuss these in detail because the corresponding CCR Census for comparison has yet to be published.

## 3.2. Comparison of Filtered META2.0 With the Subset Ring Census

The filtered (i.e., "ring-like") eddies from the global product(s) are compared to the Ring Census following the analyses conducted by Gangopadhyay et al. (2019) and Silver et al. (2021). To compare the spatial distribution of formations, we first examine formations by zone, similar to Figure 1b in Gangopadhyay et al. (2019) and Figure 1 in Silver et al. (2021). To compare the seasonality of ring formations, we average monthly formations for all zones similar to Figure 2 in Gangopadhyay et al. (2019) and Figure 3a in Silver et al. (2021). To compare the trends and test for regime shifts, we plot a time series of formations for all zones, similar to Figure 3 in Gangopadhyay et al. (2019) and Figure 2 in Silver et al. (2021). Finally, to detect a possible regime shift in the ring-like eddies, we employ the same change-point algorithm used by Gangopadhyay et al. (2019) and Silver et al. (2021), developed by Rodionov (2004). Regime shifts are defined as a rapid reorganization of a system from one stable state to another. Rodionov (2004) uses sequential *t*-tests on the mean or variance (here we used mean, as did Gangopadhyay et al. (2019) and Silver et al. (2021)) to test if the current year mean is different than the previous year mean. In short, to compare the SSH-based data product(s) filtered for ring-like eddies with the subset Ring Census, we plotted the spatial distribution (Figure 2), seasonality (Figure 3), and time series (Figure 4). We ran the regime shift detection algorithm to detect shifts in the mean annual formations of ring-like features.

PEREZ ET AL. 7 of 22

Average No. of Formations

Average No. of Formations

3

WCR

CCR-like

WCR-like

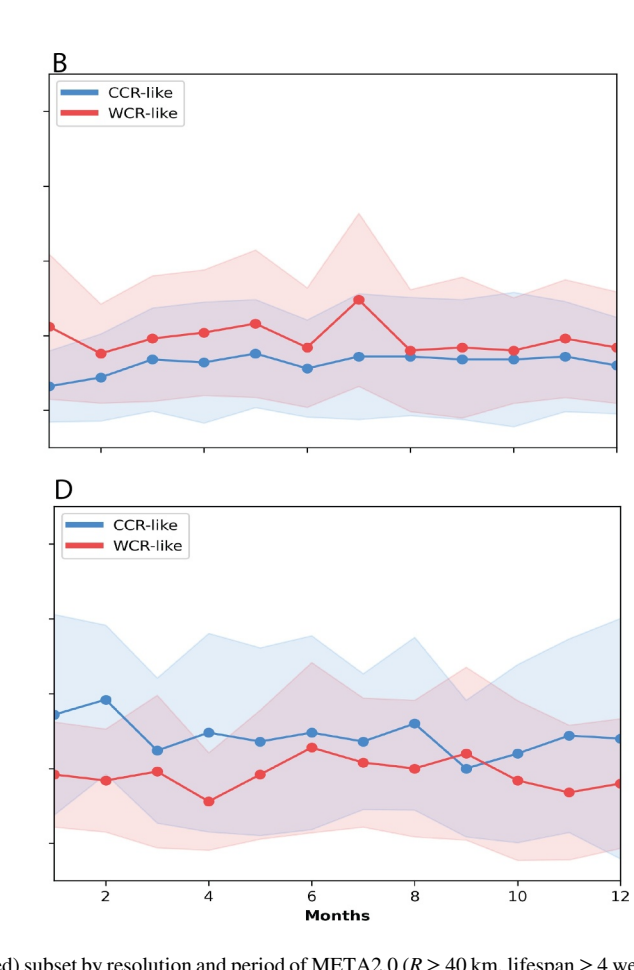


Figure 3. Seasonality of formations for (a) the Ring Census warm core rings (WCRs) (red) subset by resolution and period of META2.0 ( $R \ge 40$  km, lifespan  $\ge 4$  weeks), (b) META2.0 WCR-like eddies (red) and cold core ring (CCR)-like eddies (blue), (c) META3.1 exp WCR-like eddies (red) and CCR-like eddies (blue), and (d) GLED v1.0 WCR-like eddies (red) and CCR-like eddies (blue) with the shading denoting the standard deviation.

#### 3.3. Feature Comparisons

8

10

As a secondary analysis to compare the data products and to understand better why the products give such different results, we perform a feature-by-feature analysis for two contrasting years: 1995 and 2008. We select 1995 because (a) it was prior to the regime shift and (b) formation numbers were similar for the META2.0 WCR-like eddies (n = 11) and Ring Census WCRs (n = 11) in that year (Figure 5). We select 2008 because (a) it occurred after the regime shift and (b) formation numbers were dissimilar for the META2.0 WCR-like eddies (n = 12) and Ring Census WCRs (n = 18).

For the feature-to-feature comparison for these 2 years, we check each ring-like eddy (from META2.0) against each ring from the subset Ring Census for the given year to see if the first occurrence, that is, its "birth," is collocated in space and time. The threshold we define for two features to be collocated in space and time is (a) features are formed within 10 days of each other, (b) their centers are no more than  $0.25^{\circ}$  of latitude apart, and (c) their centers are no more than  $1^{\circ}$  of longitude apart. This threshold is based on the typical WCR translation speeds of  $0.1 \, m/s$ , which is the order of magnitude of WCR translation speeds found by Joyce (1984), Brown et al. (1986), Cornillon et al. (1989), and Silver et al. (2022). If the features in the filtered META2.0 and subset Ring Census are first identified (i.e., "born") within this threshold, we then use background SSH and SST maps for context to confirm that they are indeed the same feature.

## 3.4. Computing Energy and Speed

Daily geostrophic velocities from the Copernicus Marine Services' product Global Ocean Gridded L4 Sea Surface Heights and Derived Variables Reprocessed from 1993 to 2017 are averaged to produce monthly fields. The 25-

PEREZ ET AL. 8 of 22

21699291, 2024, 10, Downloaded from https://agupubs.onlinelibrary.wiley.com/doi/10.1029/2023JC020761 by Mbl Whoi Library, Wiley Online Library on [08/10/2024]. See the Terms and Conditions (https://onlinelibrary.wiley

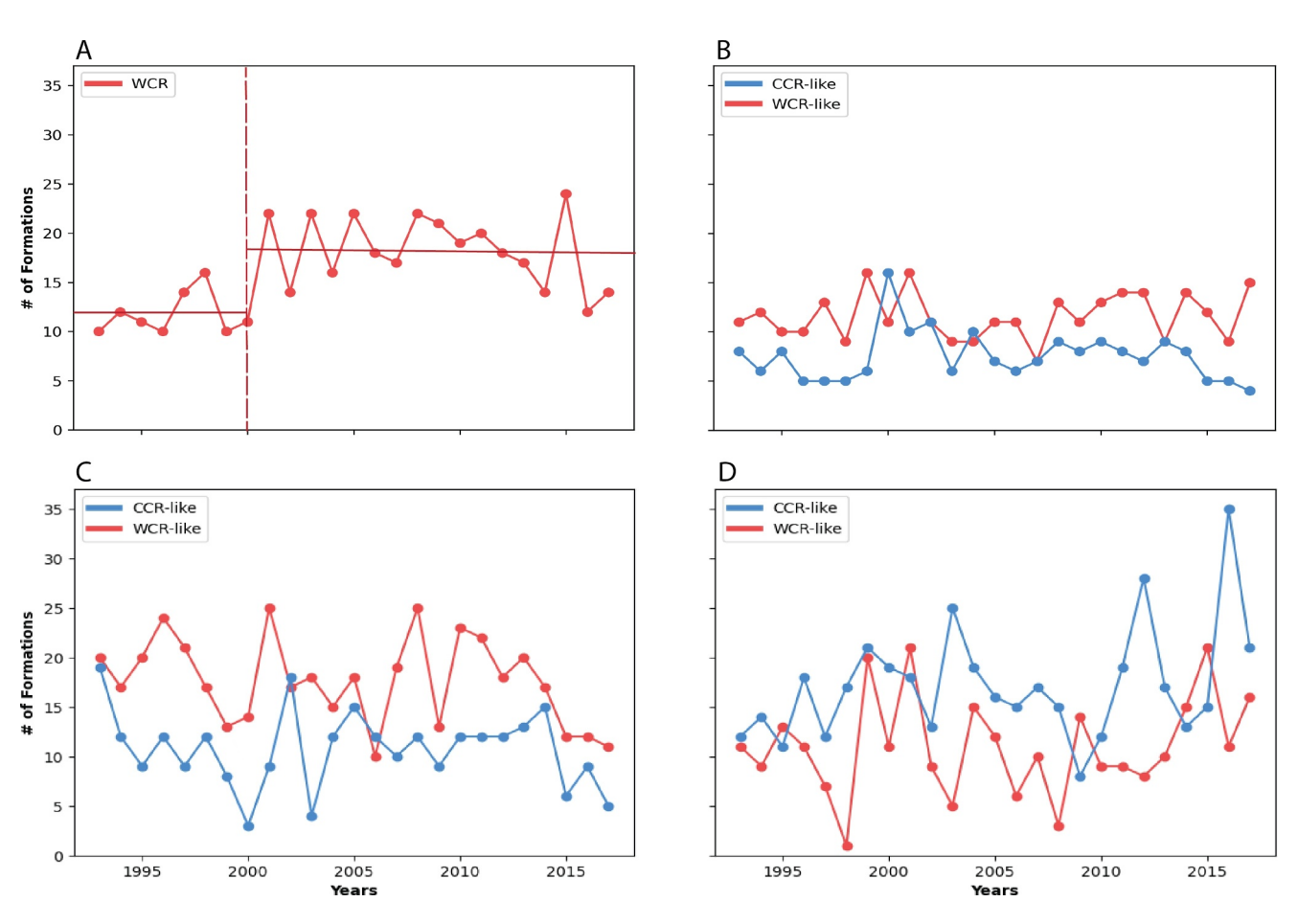


Figure 4. Annual formations for (a) the Ring Census warm core rings (WCR) (red) subset by resolution and period of META2.0 ( $R \ge 40 \text{ km}$ , lifespan  $\ge 4 \text{ weeks}$ ) with the regime shift denoted by the vertical red line at the year 2000, (b) META2.0 WCR-like eddies (red) and cold core ring (CCR)-like eddies (blue), (c) META3.1exp WCR-like eddies (red) and CCR-like eddies (blue), and (d) GLED v1.0 WCR-like eddies (red) and CCR-like eddies (blue). The only time series for which a statistically significant regime shift (p-value  $\ll 0.05$ ) was detected is the Ring Census data ( $R \ge 40 \text{ km}$ , lifespan  $\ge 4 \text{ weeks}$ ).

year monthly climatology (1993–2017) is computed for the eastward, u, and northward, v, geostrophic velocities. The EKE is computed using Equation 1, where the anomalies of geostrophic velocity are computed for each grid cell by subtracting the climatological means,  $\overline{u_c}$  and  $\overline{v_c}$ , from the monthly velocities,  $u_t$  and  $v_t$ . A reference density of  $\rho_0 = 1025 \frac{kg}{m^3}$  is used for all calculations.

$$EKE = \frac{1}{2}\rho_0 \left[ (u_t - \overline{u_c})^2 + (v_t - \overline{v_c})^2 \right] \tag{1}$$

In addition, KE is computed from monthly geostrophic velocities using Equation 2.

$$KE = \frac{1}{2}\rho_0 \overline{(u_t^2 + v_t^2)} \tag{2}$$

Speed of the surface velocities is computed from monthly geostrophic velocities using Equation 3.

$$Speed = \sqrt{u_t^2 + v_t^2} \tag{3}$$

The Northwest Atlantic region (30°N–45°N, 75°W–55°W) is considered as a whole and is also subdivided into 3 regions with boundaries that vary in time: the Slope Sea, the Gulf Stream, and the Sargasso Sea, building on the work of Bisagni et al. (2024), who computed EKE for the Slope Sea from satellite altimetry observations. In this

PEREZ ET AL. 9 of 22

21699291, 2024, 10, Downloaded from https://agupubs.onlinelibrary.wiley.com/doi/10.1029/2023JC020761 by Mbl Whoi Library, Wiley Online Library on [08/10/2024]. See the Terms and Conditions (https://online.com/doi/10.1029/2023JC020761 by Mbl Whoi Library, Wiley Online Library on [08/10/2024]. See the Terms and Conditions (https://online.com/doi/10.1029/2023JC020761 by Mbl Whoi Library, Wiley Online Library on [08/10/2024]. See the Terms and Conditions (https://online.com/doi/10.1029/2023JC020761 by Mbl Whoi Library, Wiley Online Library on [08/10/2024]. See the Terms and Conditions (https://online.com/doi/10.1029/2023JC020761 by Mbl Whoi Library, Wiley Online Library on [08/10/2024]. See the Terms and Conditions (https://online.com/doi/10.1029/2023JC020761 by Mbl Whoi Library, Wiley Online Library on [08/10/2024]. See the Terms and Conditions (https://online.com/doi/10.1029/2023JC020761 by Mbl Whoi Library, Wiley Online Library on [08/10/2024]. See the Terms and Conditions (https://online.com/doi/10.1029/2023JC020761 by Mbl Whoi Library, Wiley Online Library on [08/10/2024]. See the Terms and Conditions (https://online.com/doi/10.1029/2023JC020761 by Mbl Whoi Library, Wiley Online Library on [08/10/2024]. See the Terms and Conditions (https://online.com/doi/10.1029/2023JC020761 by Mbl Whoi Library, Wiley Online Library on [08/10/2024]. See the Terms and Conditions (https://online.com/doi/10.1029/2024).

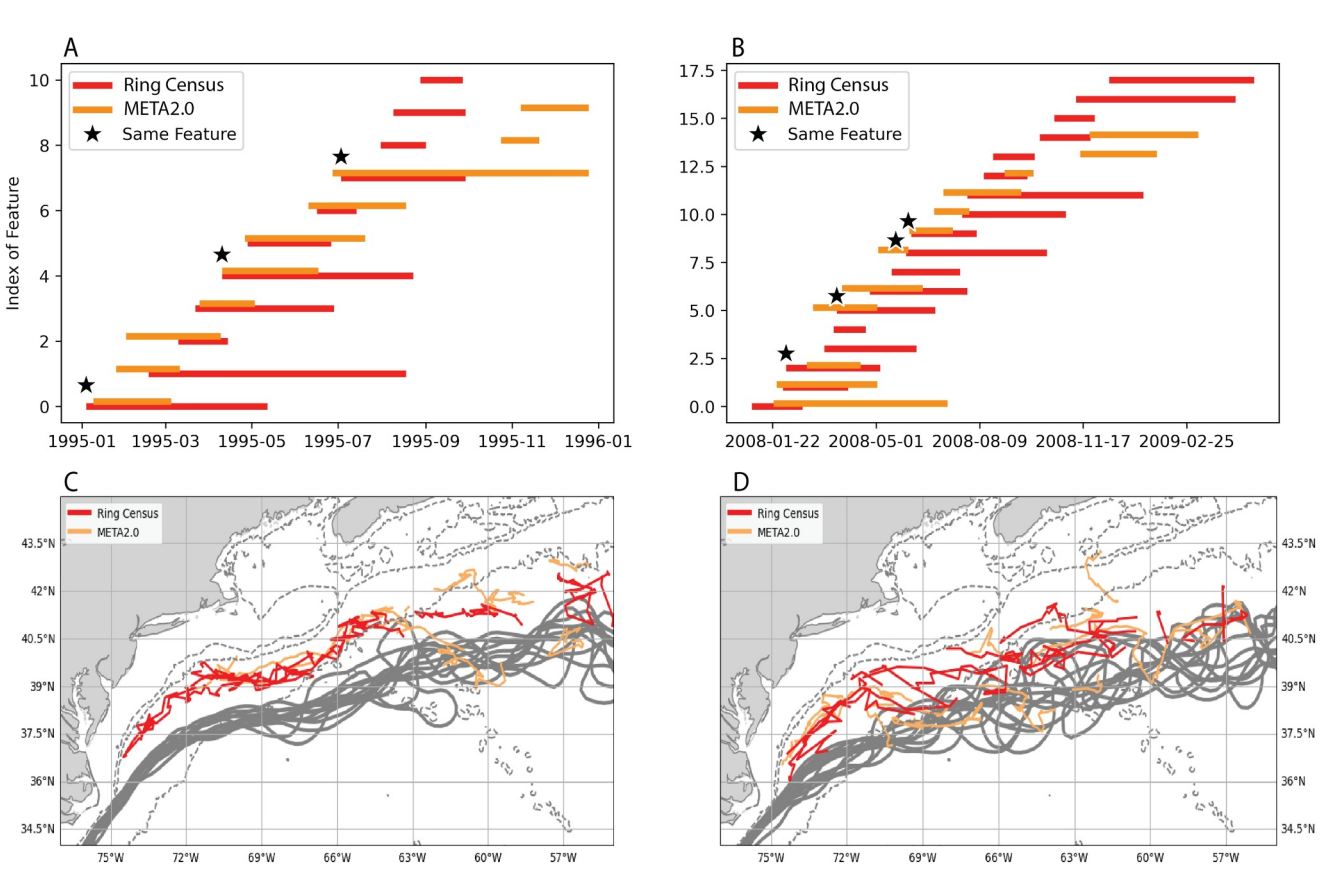


Figure 5. Feature-by-feature comparison between the subset warm core rings (WCR) ( $R \ge 40 \text{ km}$ , lifespan  $\ge 4 \text{ weeks}$ ) (red) and META2.0 WCR-like eddies (orange) for (a) 1995 and (b) 2008. The black stars in (a) and (b) denote a feature that is the same feature between both data products. All ring and eddy tracks are plotted for (c) 1995 and (d) 2008. The dashed gray lines show isobaths at 100, 1,000, and 4,000-m depth. The thick gray lines are the monthly mean Gulf Stream paths for (c) 1995 and (d) 2008.

study, the Slope Sea between 75°W and 55°W is bounded to the north by the 300-m isobath (just offshore of the shelf break) and to the south by the time-varying monthly mean Gulf Stream path identified via the 25 cm SSH contour. The Gulf Stream region between 75°W and 55°W is bounded to the north by the time-varying monthly mean Gulf Stream path identified via the 25 cm SSH contour, and to the south by the monthly mean path minus 2°, to account for the typical width of the stream (approximately 100 km) and to allow for deviations in the path that arise from a complicated, contorted Gulf Stream path. The Sargasso Sea between 75°W and 55°W is bounded to the north by the southern edge of the Gulf Stream region (as described above) and to the south by 30°N, which is the southern boundary of the Northwest Atlantic region. The areas of these time-varying regions (Slope Sea, Gulf Stream, and Sargasso Sea) and the area of the entire Northwest Atlantic, are used to calculate time series (monthly and annual averages) of the respective area-averaged quantity, for example, annual mean EKE values.

#### 4. Results

#### 4.1. Statistical Comparison

#### 4.1.1. Spatial Distribution of WCRs

In the full (unfiltered) META2.0 product, the spatial distribution of anticyclonic and cyclonic eddies monotonically increases from Zone 1 to Zone 4, with about 17% (of the 1,801) anticyclones formed in Zone 1, 26% in Zone 2, 27% in Zone 3, and 29% in Zone 4. After filtering, the formations of WCR-like eddies increase from Zone 1 (14%) through 2 (26%) and Zone 3 (31%) and then decrease in Zone 4 (29%). The distribution of formations for WCR-like eddies (Figure 2b) is similar to the WCR formation pattern found in the full Ring Census. Gangopadhyay et al. (2019) found that most WCRs are formed preferentially in Zone 3, where the New England Seamount Chain intersects the path of the Gulf Stream.

PEREZ ET AL. 10 of 22

The WCRs from the subset Ring Census (subset 1993–2017,  $R \ge 40$  km, lifespan  $\ge 4$  weeks) also exhibit this distinct distribution of zonal formations (Figure 2a) with the fewest formations in Zone 1 (9%) and increasing formations eastward to Zone 2 (25%) and Zone 3 (38%) before decreasing in Zone 4 (28%). This distribution pattern for the subset Ring Census is equivalent to that of Gangopadhyay et al. (2019) for the entire Ring Census  $\pm 5\%$ .

#### 4.1.2. Seasonality of WCR Formations

Silver et al. (2021) reported asymmetric seasonal cycles for WCRs and CCRs, with CCR formation peaking in May and WCR formation peaking in July. The subset WCRs have the same seasonality found in Gangopadhyay et al. (2019) and Silver et al. (2021) (Figure 3a). This strong seasonal cycle is characterized by minimum formations in the winter (January and December), an increase of formations during the spring, peak formations in July, and a decrease in the fall (Figure 3). Although the absolute number of formations is lower for the subset WCRs, we see the same seasonal cycle pattern originally found by Gangopadhyay et al. (2019) and Silver et al. (2021). The seasonality reported in Silver et al. (2021) is consistent with the model results of the seasonal EKE of the Gulf Stream from Kang et al. (2016).

In contrast, there is no apparent seasonal signal for the WCR-like eddies (Figure 3b). Additionally, there is little to no variability in the number of monthly formations, with the standard deviations being on the same order as the magnitude of formations per month (Figure 3b). The finding that the META2.0 filtered product has no discernible seasonality, a robust finding of Silver et al. (2021) that is corroborated by the model results of Kang et al. (2016), suggests that these data products may capture entirely different features.

#### 4.1.3. Regime Shift Detection

The key finding of Gangopadhyay et al. (2019), expanded upon by Silver et al. (2021), is the occurrence of a regime shift in 2000. While we do find a regime shift in the subset WCRs (Figure 4a), we do not detect it in the WCR-like eddies (Figure 4b). The subset WCRs averaged 12 formations before 2000 (1993–1999) and 18 formations after 2000 (2000–2017). This result is not quite as striking as the regime shift in 2000 from the full Ring Census data product, which indicated a doubling in formations (Gangopadhyay et al., 2019; Silver et al., 2021), but still includes a substantial increase in formations in the year 2000. When we employ the same regime shift detection algorithm that Gangopadhyay et al. (2019) and Silver et al. (2021) used, we still find a significant regime shift around  $2000 \, (p\text{-value} \ll 0.05)$  for the subset WCRs. Depending on the cut-off period, the regime shift year in the subset data is either 2000 for a cut-off period of 5–8 years or 2001 for 9–12 years. When we employ the regime shift detection algorithm on the WCR-like eddies, we do not detect any regime shifts.

## 4.1.4. Examination of META3.1exp and GLED v1.0

The new eddy products, META3.1exp and GLED, may offer some improvements in eddy-detection schemes relative to META2.0, but as described below, they still do not capture the essential characteristics of WCR formations identified with the Ring Census. Hence, they are not better suited than META2.0 for studying Gulf Stream rings. In the (filtered) META3.1exp product, the WCR-like eddy formations increase monotonically eastward from Zone 1 to Zone 4 (Figure 2c), there is no discernible seasonality in formations (Figure 3c), nor is a regime shift detected (Figure 4c). There are two key differences between this product and the META2.0 eddies. First, the filtered META3.1exp ring-like eddies product identifies almost twice as many formations as the filtered META2.0 product. Second, META3.1exp WCR-like eddy formations peak in Zone 4, not Zone 3, as META2.0 and Ring Census WCRs do (Figure 2).

The GLED v1.0 product WCR-like eddy formation count is similar to META2.0 and the Ring Census. However, the pattern of formations is shifted one Zone to the west, with formations peaking in Zone 2 (Figure 2d). There is no discernible seasonality to GLED v1.0 ringlike eddy formations (Figure 3d), and no regime shift is detected (Figure 4d). The formation pattern of GLED v1.0 WCR-like eddies does not match the pattern found by Gangopadhyay et al. (2019) and Silver et al. (2021) (Figure 2), which showed that the peak in formations in Zone 3 is consistent with established seasonality of EKE in the Northwest Atlantic (Kang et al., 2016; Zhai et al., 2008). Overall, the new products are no more consistent with the Ring Census results than META2.0, so our feature-by-feature comparison (Section 4.2) focuses on comparing filtered META2.0 and the subset Ring Census to explore the difference in results.

PEREZ ET AL. 11 of 22

**Table 2**Summary of Features for All Data Products Collocated in Space and Time With Subset Warm Core Rings From Ring Census (1993–2017)

	Ring Census	META2.0	META3.1exp	GLED v1.0
WCRs or WCR-like eddies	406	320	429	276
WCR-like eddies matched	-	26	43	17
Percent match (%)	-	9	9	6

## 4.2. Feature-By-Feature Comparisons

To investigate why the META2.0 WCR-like eddies do not show seasonality in formations (Figure 3b) nor evidence of a regime shift (Figure 4b), we perform a detailed comparison of the eddy identifications and tracking for 2 years, 1995 and 2008. We compare the WCRs with WCR-like eddies with one another, using mapped SSH and SST for context. These years are chosen to examine the periods before and after the regime shift. Furthermore, 1995 had the same number of formations for the subset WCRs (n = 11) and the WCR-like eddies (n = 11), while 2008 had a dissimilar number of formations for the subset WCRs (n = 18) and the WCR-like eddies (n = 12).

Careful inspection to identify collocated features (see Methods, Section 3) indicates that while both data products identified 11 features in 1995, only 3 (27%) features were the same (starred features in Figure 5a). Even between these three common features, there was a substantial difference in the identification and tracking. The first feature of 1995 was identified in the Ring Census five days before the META2.0 algorithm identified it. The second feature was identified on the same day by both. The third feature was identified by the META2.0 algorithm 6 days before the Ring Census identified it. This third and final feature was identified in July when the SST difference between WCRs and ambient Slope Sea waters is typically reduced due to heat fluxes that warm the entire region. This seasonal warm cap can make it difficult to identify rings in SST images. The META2.0 algorithm followed the feature for 6 months, and the Ring Census recorded the same feature for 2 months. In 2008, there were 12 formations of META2.0 WCR-like eddies, whereas the subset Ring Census ( $R \ge 40$  km, lifespan  $\ge 4$  weeks) recorded 18 formations. We find that 4 of the 12 (33%) features were the same (starred features in Figure 5b). In all of the cases, the Ring Census identified WCRs a few days before their SSH contours closed, and before the META2.0 algorithm was able to identify them. Both data products only identified about one-third of the features to be the same (27% in 1995 and 33% in 2008).

Motivated by these year-to-year case studies, we checked all META2.0 WCR-like eddies against subset WCRs to calculate how many features were collocated in space and time (Table 2). As noted previously, to consider a feature collocated in time and space, we check that the first occurrences are within 10 days of each other, their centers are no more than  $0.25^{\circ}$  latitude apart, and no more than  $1^{\circ}$  longitude apart (assuming about  $0.1 \ m/s$  translation speed). With these criteria, 26 out of 320 (9%) WCR-like eddies match subset WCRs. These results indicate a lower agreement in the feature-to-feature calculation than the year-to-year case studies, 27% for 1995 and 33% for 2008. A less restrictive window for collocation (formed within 10 days of each other, their centers are no more than  $0.25^{\circ}$  latitude apart, and no more than  $10^{\circ}$  longitude apart, translation speed  $1 \ m/s$ ) still yields similarly low percentages for a match-up of features: 54 of 320 (16% of features). When we compute the number of collocated features for META3.1exp and GLED v1.0 WCR-like eddies to the subset WCRs, we find 43 of 429 (9%) META3.1exp features match and 17 of 276 (6%) GLED v1.0 features match (Table 2).

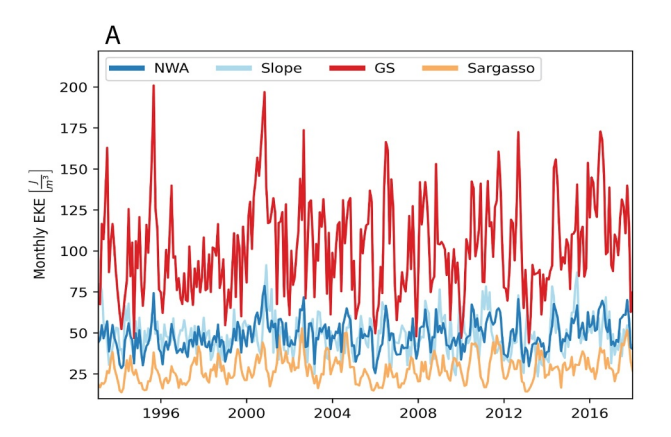
## 4.3. Energy and Speed

Though the global eddy products have difficulty distinguishing Gulf Stream rings from other eddy activity and are therefore not able to capture the observed regime shift in WCRs, a notable change in the state of the Northwest Atlantic in the year 2000 is evident in the satellite altimetry-derived EKE (Figures 6 and 7), KE (Figure 8c), and speed of geostrophic surface velocities (Figures 8a and 8b). The spatially averaged time-mean EKE prior to 2000 (1993–1999) is  $44.5 \, \text{J/m}^3$ , while that after 2000 (2000–2017) increases to  $50.1 \, \text{J/m}^3$  (Figure 7). A change-point analysis of the annual EKE time series averaged over the Northwest Atlantic shows a statistically significant regime shift at 2000 (p-value = 0.0013, Figure 6b).

PEREZ ET AL. 12 of 22

21699291, 2024, 10, Downloaded from https://agupubs.onlinelibrary.wiley.com/doi/10.1029/2023JC020761 by Mbl Whoi Library, Wiley Online Library on [08/10/2024]. See

onditions) on Wiley Online Library for



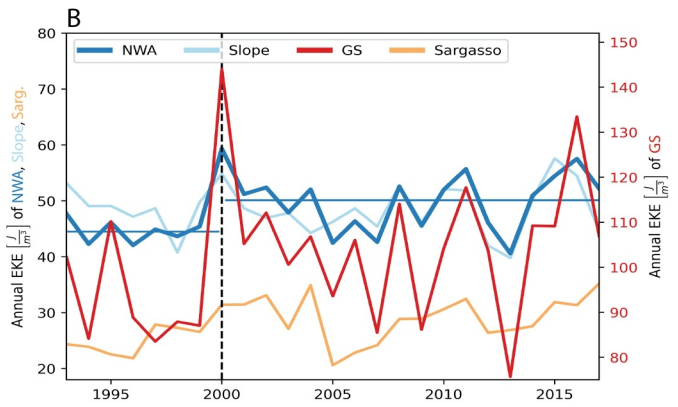


**Figure 6.** The spatially averaged eddy kinetic energy (EKE) (Equation 1, units  $J/m^3$ ) per unit volume in the Northwest Atlantic region (30°N–45°N, 85°W–55°W) from 1993 to 2017 computed relative to a 25-year climatology (1993–2017) is plotted for the (a) monthly and (b) annual averages. The Northwest Atlantic is decomposed into 4 components: the whole region (dark blue), the Slope Sea (light blue), the Gulf Stream (red), and the Sargasso Sea (orange). The shift to a higher EKE state in the entire Northwest Atlantic region is indicated by the black vertical dashed line and the blue horizontal lines in panel (b) that represent the mean, spatially averaged EKE for the whole system before 2000, 44.5  $J/m^3$ , and after 2000, 50.1  $J/m^3$  (p-value = 0.0013). The y-axes of (b) have different ranges due to the higher values of EKE in the Gulf Stream region. In (b), all regions' EKE values are plotted on the left y-axis and the EKE of the Gulf Stream is plotted on the right y-axis to show the variability of all regions clearly.

The annual Northwest Atlantic EKE time series exhibits not only a shift to a higher EKE state after 2000, which is identified by the regime shift analysis (p-value = 0.0013, Figure 6b), but also exhibits higher variance in the EKE after 2000 (Figure 6a). As previously mentioned, the EKE time series of the Northwest Atlantic (30°N–45°N, 75° W–55°W) is separated into 3 subregions: the Slope Sea (75°W–55°W, the 300-m isobath to the north, and the Gulf Stream monthly path to the south), the Gulf Stream (75°W–55°W, the Gulf Stream monthly mean path to the north and 2°S of the time-varying path as the southern boundary), and the Sargasso Sea (75°W–55°W, the bottom boundary of the Gulf Stream region to the north, and 30°N as the southern boundary). The shift to a higher EKE state after 2000 is most pronounced in the Gulf Stream region.

A shift to a higher energy state in the Northwest Atlantic from prior to 2000 (1993–1999) and after 2000 (2000–2017) is evident in the spatially averaged EKE and KE (Figures 7 and 8). The shift is also evident in the spatial distribution of speeds prior to 2000 (Figure 8a) relative to those after 2000 (Figure 8b), as highlighted in the difference in KE between these two time periods (Figure 8c). Spatially, the greatest changes in EKE, KE, and speed are located along the Gulf Stream main axis; particularly in the region where the mean Gulf Stream path crosses the New England Seamount Chain in Zones 2 and 3 (70°W–65°W and 65°W–60°W) (Figures 7c and 8c). The largest decrease in the EKE, KE, and speed occurs north of the mean Gulf Stream path and east of 70°W, particularly in Zone 4 (60°W–55°W). Additionally, an increase in the KE and speed is evident in the western Slope Sea north of the Gulf Stream mean path between 70°W and 65°W.

## 5. Discussion

## 5.1. Statistical Comparison

Despite the similarity in the spatial distribution of WCR formations noted between the subset (and full) Ring Census and META2.0 (Figures 2a and 2b), the seasonality and the other details of WCR formations indicate that the same features are not being identified across data products. The META2.0 product identifies 3,371 eddies in the region (30°N–45°N, 75°W–55°W) from 1993 to 2017. In contrast, the Ring Census identifies only 961 WCRs from 1980 to 2017. From our feature-by-feature analysis and collocation calculation, we know that most of those >3,000 eddies are not relevant for studying Gulf Stream rings but rather represent other coherent eddies (not formed from the Gulf Stream) or mesoscale variability that is not associated with a coherent, swirling feature. Hence, there is a need to filter the META2.0 eddies to produce WCR- and CCR-like eddies. However, even after this filtering, the META2.0 eddy product does not identify a majority of the same features as identified by the Ring Census.

PEREZ ET AL. 13 of 22

21699291, 2024, 10, Downloaded from https://agupubs.onlinelibrary.wiley.com/doi/10.1029/2023/C020761 by Mbl Whoi Library, Wiley Online Library on [08/10/2024]. See the Terms and Conditions (https://onlinelibrary.wiley.com/terms-and-conditions) on Wiley Online Library for rules of the Terms and Conditions (https://onlinelibrary.wiley.com/terms-and-conditions) on Wiley Online Library for rules of the Terms and Conditions (https://onlinelibrary.wiley.com/terms-and-conditions) on Wiley Online Library for rules of the Terms and Conditions (https://onlinelibrary.wiley.com/terms-and-conditions) on Wiley Online Library for rules of the Terms and Conditions (https://onlinelibrary.wiley.com/terms-and-conditions) on Wiley Online Library for rules of the Terms and Conditions (https://onlinelibrary.wiley.com/terms-and-conditions) on Wiley Online Library for rules of the Terms and Conditions (https://onlinelibrary.wiley.com/terms-and-conditions) on Wiley Online Library for rules of the Terms and Conditions (https://onlinelibrary.wiley.com/terms-and-conditions) on Wiley Online Library for rules of the Terms and Conditions (https://onlinelibrary.wiley.com/terms-and-conditions) on Wiley Online Library for rules of the Terms and Conditions (https://onlinelibrary.wiley.com/terms-and-conditions) on Wiley Online Library for rules of the Terms and Conditions (https://onlinelibrary.wiley.com/terms-and-conditions) on Wiley Online Library for rules of the Terms and Conditions (https://onlinelibrary.wiley.com/terms-and-conditions) on Wiley Online Library for rules of the Terms and Conditions (https://onlinelibrary.wiley.com/terms-and-conditions) on Wiley Online Library for rules of the Terms and Conditions (https://onlinelibrary.wiley.com/terms-and-conditions) on Wiley Online Library for rules of the Terms and Conditions (https://onlinelibrary.wiley.com/terms-and-conditions) on Wiley Online Library for rules of the Terms and Conditions (https://onlinelibrary.wiley.com/terms-and-conditions) on Wiley Online Library for rules of the Terms

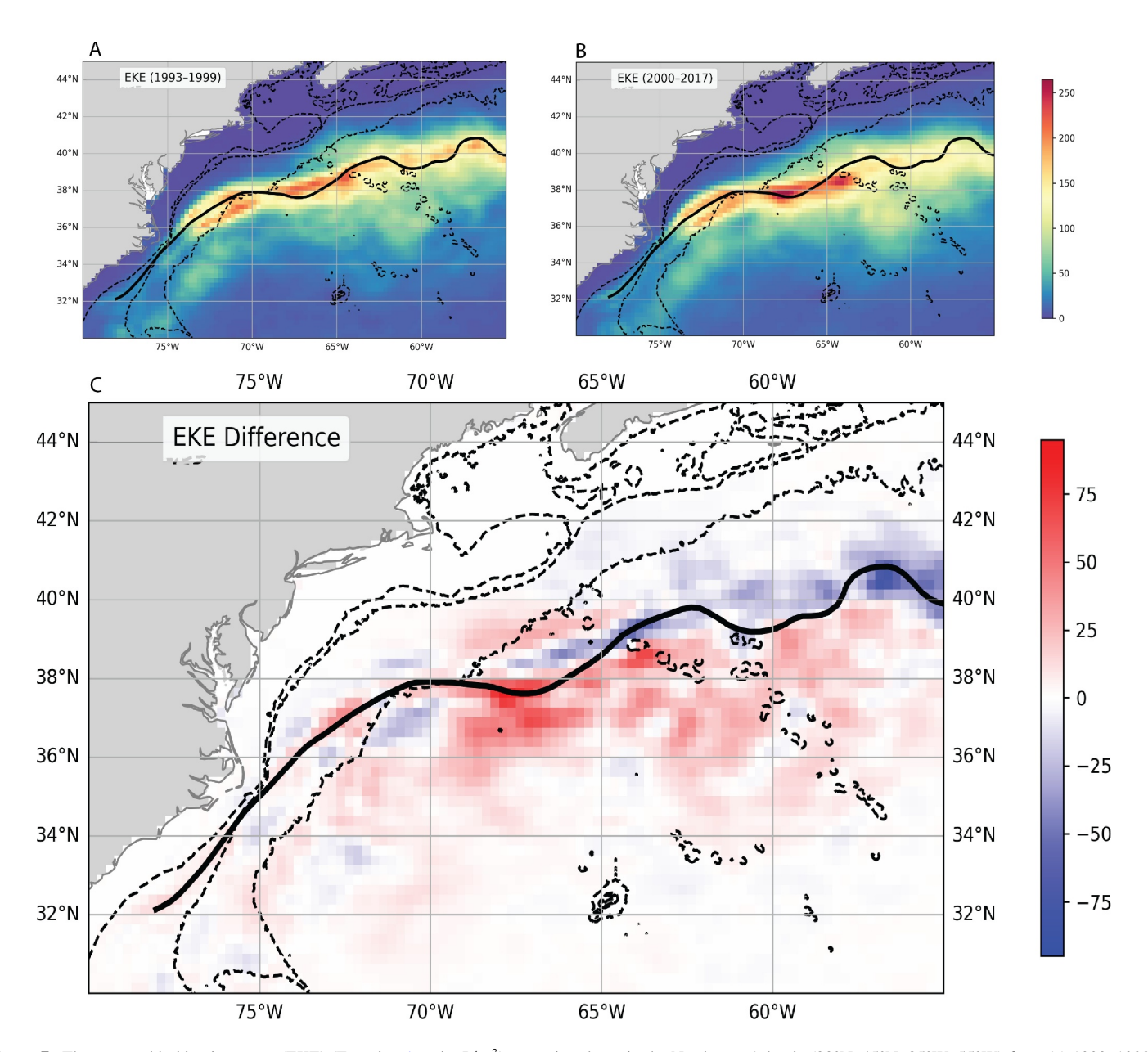


Figure 7. The mean eddy kinetic energy (EKE) (Equation 1, units  $J/m^3$ ) per unit volume in the Northwest Atlantic (30°N-45°N, 85°W-55°W) from (a) 1993–1999 computed relative to a 25-year climatology (1993–2017) is compared to (b) the mean EKE per unit volume in the Northwest Atlantic from 2000 to 2017 computed relative to the same climatology. The difference between (a and b) is highlighted in (c), which shows EKE from 2000 to 2017 minus EKE from 1993 to 1999. In (c), the red shading (positive) indicates an increase in EKE during the post-2000 period (2000–2017) relative to the pre-2000 period (1993–1999), and the blue shading (negative) indicates a decrease in EKE in the post-2000 period relative to the pre-2000 period. The thick black line is the mean Gulf Stream path 1993–2022 identified via the 25 cm sea surface height contour is plotted for reference. The thin black, dashed lines show isobaths at 100, 1,000, and 4,000-m depth.

The filtered (and unfiltered) META2.0 product also does not capture the observed seasonality of WCR or CCR formations. The seasonality of EKE in the Gulf Stream area has been well-established to be higher in the summer and a minimum in the winter (Kang et al., 2016; Zhai et al., 2008). The META2.0 WCR-like eddies do not capture this robust feature of variability. Finally, the META2.0 product has no regime shift in WCR-like eddies. Due to the temporal and spatial resolution of the merged SSH fields, the META2.0 algorithm cannot detect shorter-lived rings. The fundamental differences in methodology might explain why global eddy products identify different features, and it is necessary to examine these products in the context of auxiliary data to determine where the various products have applicability in the vicinity of western boundary currents.

PEREZ ET AL. 14 of 22

21699291, 2024, 10, Downloaded from https://agupubs.onlinelibrary.wiley.com/doi/10.1029/2023JC020761 by Mbl Whoi Library, Wiley Online Library on [08/10/2024]. See the Terms and Conditions (https://onlinelibrary.wiley

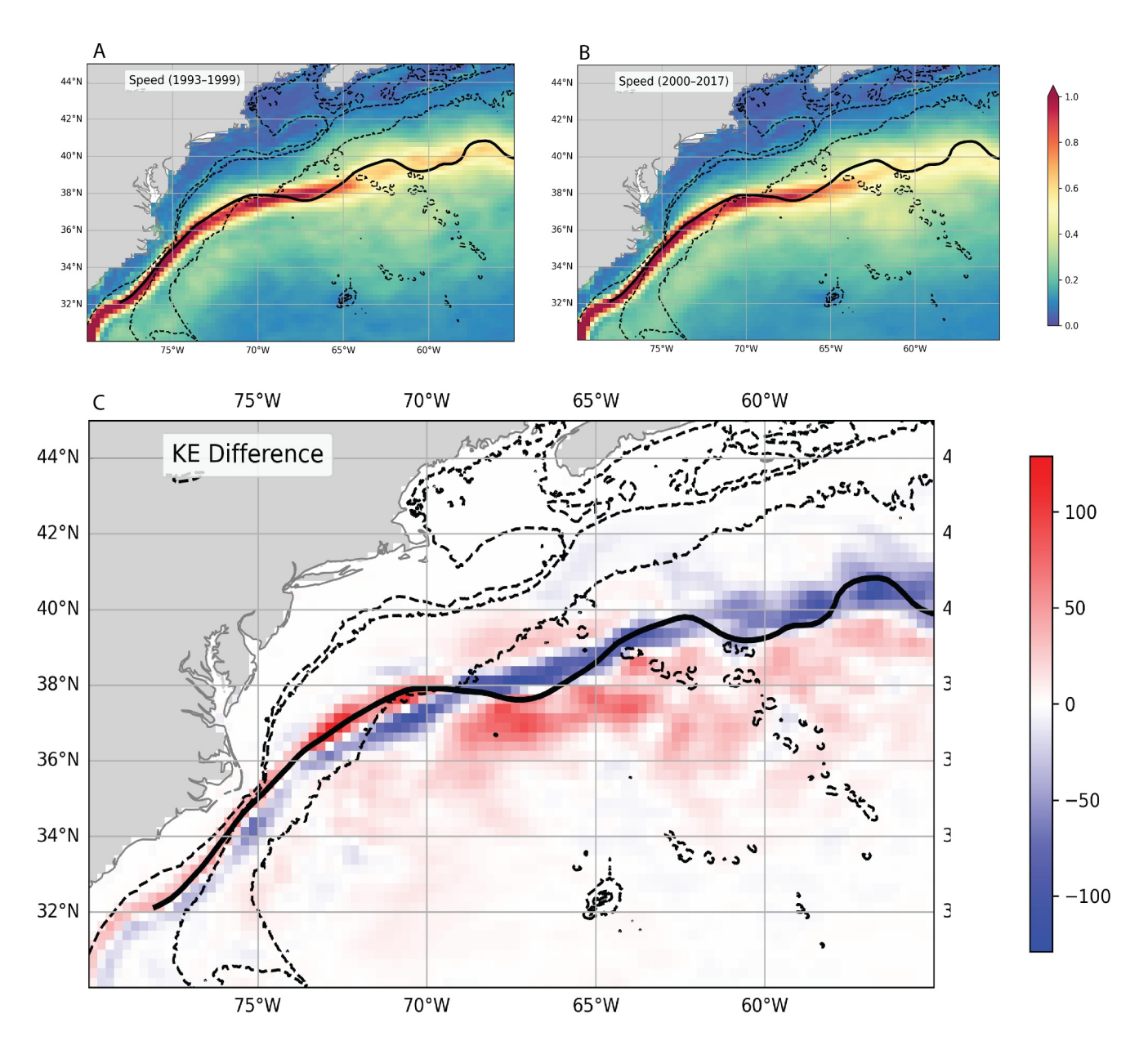


Figure 8. The mean surface speed (Equation 3, units  $\frac{m}{s}$ ) of the Northwest Atlantic (30°N–45°N, 85°W–55°W) from (a) 1993–1999 is compared to (b) the mean surface speed  $\left(\frac{m}{s}\right)$  from 2000 to 2017. The difference between (a and b) is highlighted by (c) which shows the difference in the spatially averaged kinetic energy (KE) (Equation 2, units J/m³) per unit volume of the Northwest Atlantic from 1993 to 1999 minus 2000 to 2017. In (c), the red shading (positive) indicates an increase in KE during the post-2000 period (2000–2017) relative to the pre-2000 period (1993–1999), and the blue shading (negative) indicates a decrease in KE in the post-2000 period relative to the pre-2000 period. The thick black line is the Gulf Stream averaged path identified via the 25 cm sea surface height contour from 1993 to 2022, plotted for reference. The thin black, dashed lines show isobaths at 100, 1,000, and 4,000-m depth.

#### 5.2. Feature-By-Feature Comparison

The year-by-year case study for 1995 and 2008 reveals that META2.0 identifies about one-third, or less, of the same features identified in the Ring Census. Of the 23 features examined for the two years, only 7 are clearly the same feature. Out of these 7 matched features, there is one instance in which the META2.0 algorithm identifies a ring before the Ring Census and tracks it for longer. We further examine this feature to demonstrate how the differences in data and methodology lead to different results when identifying and tracking what is ostensibly the "same" feature (Figures 9 and 10).

PEREZ ET AL. 15 of 22



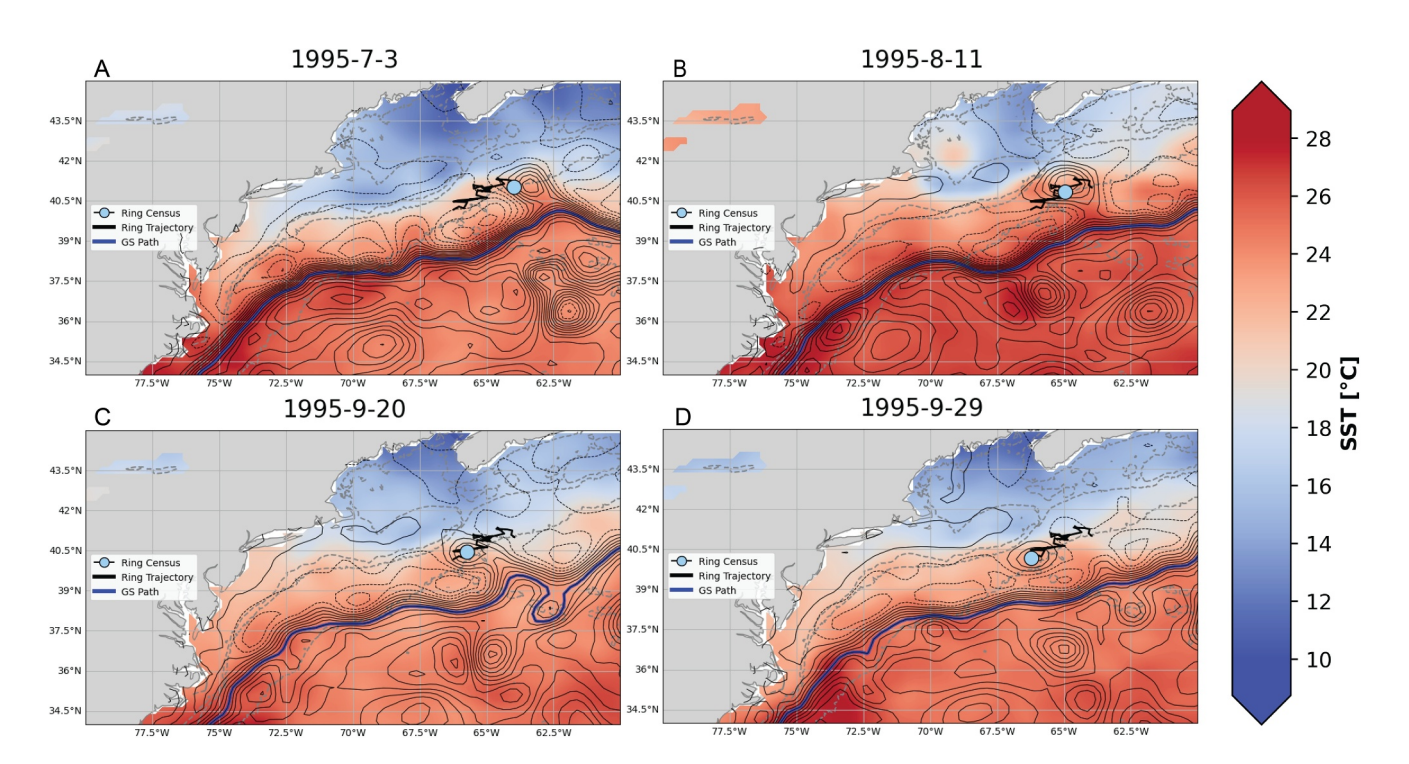


**Figure 9.** The evolution of a warm core ring (WCR) from the Ring Census in July 1995 is shown at four stages. (a) The ring was first identified in July 1995 near 41°N, 64°W, and moves westward. (b) The ring appears to start to interact with the northern wall of the Gulf Stream in August 1995 around 41°N, 65°W. (c) The sea surface height (SSH) bridge that connected the ring to the Gulf Stream starts to diminish near 40°N, 66°W. (d) The ring is last identified on 29 September 1995. The SSH bridge to the Gulf Stream has disappeared. The background color shading indicates sea surface temperature, the thin black contours are the absolute dynamic topography of SSH, and the thick black line is the trajectory of the feature. The light blue circle is the center of the WCR on the given day, and the thick blue line is approximately the Gulf Stream path, identified by the 25 cm SSH contour.

First, we consider the evolution of the ring as depicted by the Ring Census trajectory (Figure 9). This particular feature is first identified by the Ring Census on 3 July 1995 (Figure 9a) and meets its demise on 29 September 1995 (Figure 9d), about a 3-month lifespan. During this 3-month period, the ring takes a complicated path that is approximately southwestwards. In August 1995, an SSH bridge starts to form between the ring and the Gulf Stream (Figure 9b). The ring starts to separate again from the Gulf Stream in September (Figure 9c). A few days later, in September 1995, the ring demises (Figure 9d).

Now, we consider the evolution of the same ring as depicted by the META2.0 trajectory (Figure 10). This particular WCR-like eddy is first identified in META2.0 on 27 June 1995 (Figure 10a) and meets its demise on 25 December 1995 (Figure 10d), about a 6-month lifespan—3 months longer than the same feature tracked in the Ring Census. This WCR-like eddy takes a relatively straight path (compared to Figure 9) southwestwards. In August 1995, the same SSH bridge forms between the WCR-like eddy and the Gulf Stream (Figure 10b). The WCR-like eddy starts to separate again from the Gulf Stream in September (Figure 10c). A few days later, in September 1995, the WCR-like eddy is no longer attached to the Gulf Stream via the SSH bridge (Figure 10d). This WCR-like eddy continues to propagate for 3 months longer than the ring identified by the Ring Census.

When we consider why the same feature is tracked differently by the two products, we consider observations that each product primarily relies on. This feature is identified in July 1995 when temperatures throughout the Slope Sea are relatively warm so that it can be difficult to identify the SST signature of a WCR. In contrast, META2.0 is better able to track the feature continuously since ring identification relies on SSH, which is not seasonally obscured. An alternative explanation for the difference in detection and tracking of this ring may be that the Ring Census considered this ring a reabsorption back into the Gulf Stream (Figure 9d). When the feature separated again, it would have been considered a new ring, unlike the META2.0 algorithm that considered this one feature (possibly due to the low horizontal resolution of SSH maps, which could not resolve a reabsorption). This case study demonstrates that there are many ways in which the identification and tracking can differ and gives some insight into why only 9% of the META2.0 features are collocated in space and time with the Ring Census WCRs;

PEREZ ET AL. 16 of 22

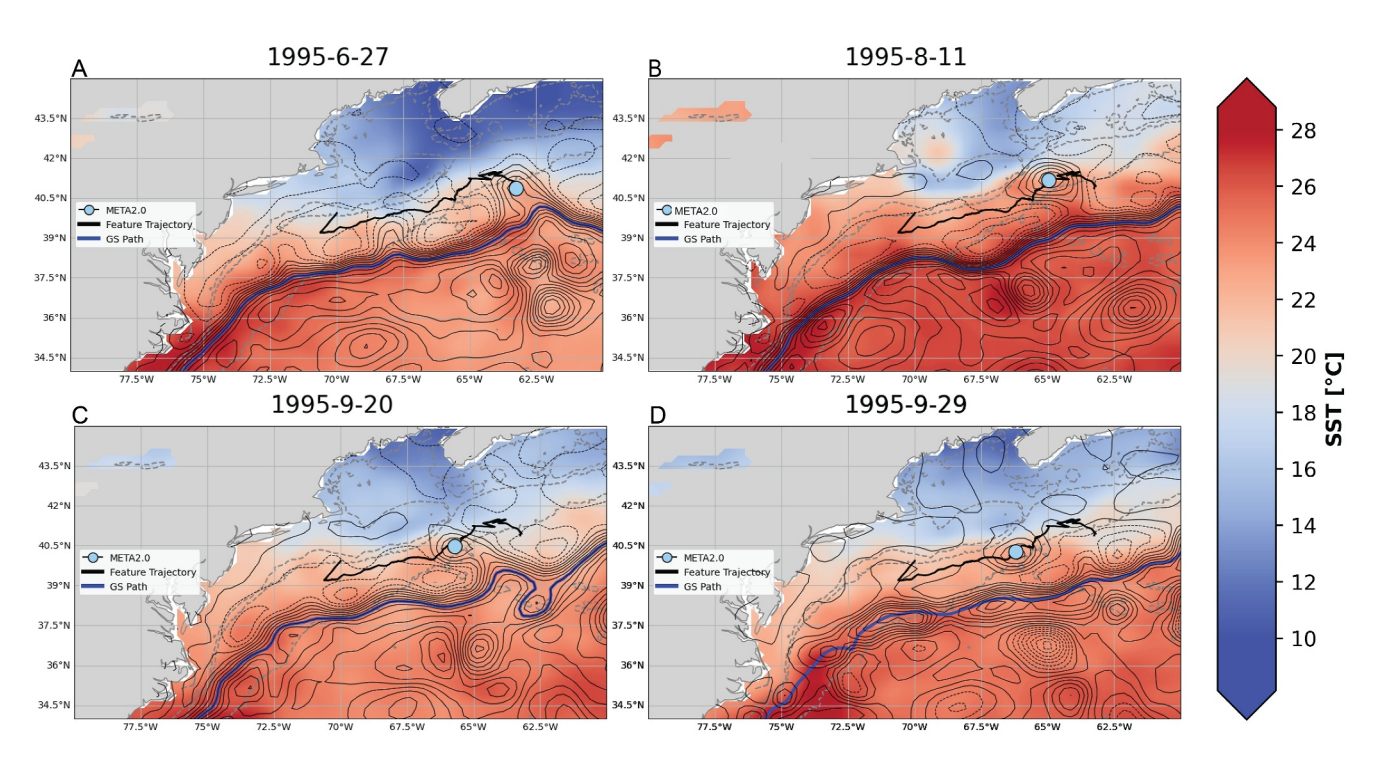


Figure 10. The evolution of a warm core ring (WCR)-like eddy from the META2.0 data product (matched to the July 1995 WCR from the Ring Census) is shown at four stages. (a) The eddy was first identified a few days before the ring in June 1995 near 41°N, 64°W. (b) The ring moves westward to about 41°N, 65°W, and an sea surface height (SSH) bridge to the Gulf Stream starts to form in August 1995. (c) The eddy is still connected to the Gulf Stream via an SSH bridge on 20 September 1995 near 40°N, 65°W. (d) The SSH bridge has disappeared, and the META2.0 WCR-like eddy continues to be tracked for 4 more months to December 1995 at its demise near 40°N, 70°W. The background color shading indicates sea surface temperature, the thin black contours are the absolute dynamic topography of SSH, and the thick black line is the trajectory of the feature. The light blue circle is the center of the ring on the given day, and the thick blue line is approximately Gulf Stream path, identified by the 25 cm SSH contour.

the differences in the seasonality and resolution of the base data (SST vs. SSH) and in the methodology clearly lead to different results.

Conversely, we show an instance in which a WCR from the Ring Census lives longer than 4 weeks and has a radius greater than 40 km (lifespan 26 weeks, R = 84 km) in Figure 11. In theory, this ring is long-lived and large enough to be identified by the META2.0 algorithm. As we follow its evolution in time, we observe that the closed SSH contours associated with the feature are transient. In the 6.5 lifespan of the ring, in some snapshots the ring is clearly located in the center of closed SSH contours, and in other snapshots the ring is not associated or contained with any closed SSH contours. What we observe is that the transition of the ring from contained within closed SSH to no closed SSH contours in less than a month. The META2.0 algorithm requires a feature to have closed SSH contours for at least 4 weeks, in order to start to be tracked.

We highlight two instances in which the tracked ring is contained in closed SSH contours and then 4 weeks later is no longer associated with closed SSH contours. In Figure 11a, the ring is contained within tight, concentric closed contours, indicating a stronger SSH gradient around the ring, which is expected since this feature is shown 3 weeks after its birth. Then, in Figure 11b, 4 weeks later than Figure 11a, the ring has moved westwards but is no longer contained in any closed SSH contours. A similar evolution is shown in Figures 11c and 11d, about 3.5 months later. In Figure 11c the ring is, again, centered in closed SSH contours, although these contours are not as tight, indicating the SSH gradient around the ring is not as strong as it was months ago in Figure 11a. Then, 1 month later in Figure 11d, the feature is no longer contained in closed SSH contours. The transient nature of the closed SSH contours associated with this ring are an example of how a feature might be identified in the Ring Census from other data, but throughout the evolution of that feature it may not be identified and tracked by an eddy tracking algorithm such as the META2.0 algorithm.

These data products each have inherent limitations that impact their applicability to statistical studies of Gulf Stream rings. One of the critical components of defining a ring is the difference between its rotational speed and

PEREZ ET AL. 17 of 22



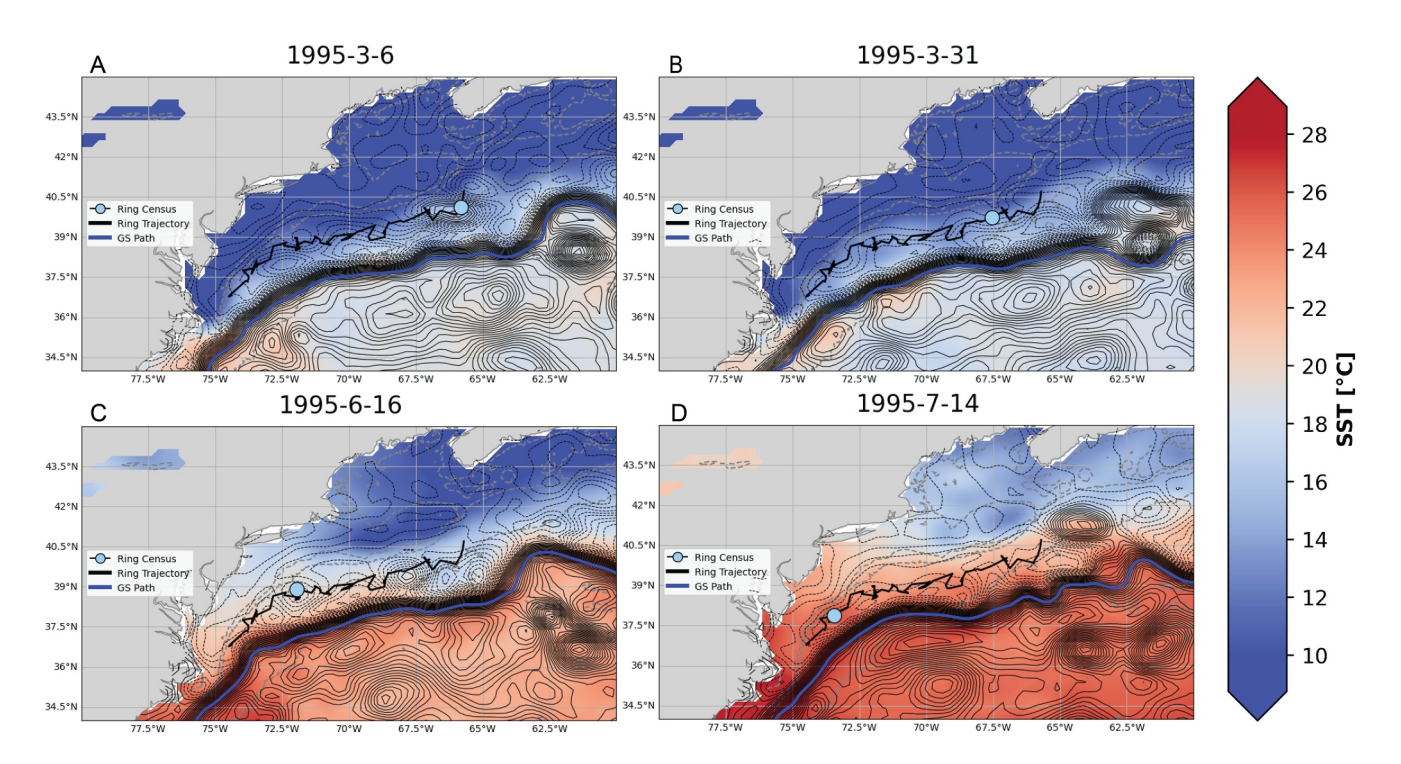


**Figure 11.** The evolution of a warm core ring (WCR) from the Ring Census born in February 1995 is shown at four stages. The ring was first identified in February 1995 near 40.5°N, 65.5°W, and moves southwestwards initially and then westwards in early March 1995 where it is shown in (a) in closed sea surface height (SSH) contours. (b) The ring moves further west by late March 1995, but is no longer contained in closed SSH contours, compared to about 1 month prior, shown in panel (a). (c) Three months later in mid-June 1995 the ring has moved westwards to 39°N, 72°W, and is contained in closed SSH contours as it nears the end of its trajectory close to the shelf break. (d) One month later in mid-July 1995 the ring has moved further southwestwards to 38°N, 73°W, somewhat parallel to the shelf break, but it is no longer associated with closed SSH contours. The background color shading indicates sea surface temperature, the thin black contours are the absolute dynamic topography of SSH, and the thick black line is the trajectory of the feature. The light blue circle is the center of the WCR on the given day, and the thick blue line is approximately the Gulf Stream path, identified by the 25 cm SSH contour.

translational speed, which serves as an indicator of whether the feature has trapped fluid in its core. Theoretically, the rotational speed should be greater than the translational speed to trap the warm fluid in its core and move it with it as it translates. This criterion cannot be evaluated for a ring without velocity data; the lack of velocity data for the Ring Census is an important limitation for ring studies.

A study by Lambhate et al. (2021) used a deep convolutional neural network trained on SST, SSH, and manual feature annotation to identify the Gulf Stream and rings. It identified rings with 71% accuracy compared to the annotated Clark charts, which the Ring Census is based on. While this 71% eddy identification accuracy is much higher than the 9% match of features found here in the subset Ring Census and META2.0 (using a simple threshold on the collocation of features in space and time), the neural network still misses about 30% of features captured by the Ring Census, even though it capitalized on both SSH and SST observations.

Even the newest products (META3.1 and GLED v1.0), filtered for ring-like eddies, give results that are inconsistent with the existing Ring Census studies, suggesting that the SSH-based products are not appropriate for statistical studies of Gulf Stream rings. Indeed, Chelton et al. (2011) acknowledge that imperfectly identified eddies are most common in regions with energetic mesoscale variability, for example, Western Boundary Current regions. Liu and Abernathey (2023) make note of the limited number of rotationally coherent Lagrangian vortices (also called Lagrangian eddies) along the main axis of western-boundary currents, which differs from the broad distribution of SSH eddies in products such as META2.0. Both new products use Absolute Dynamic Topography fields to better detect and track eddies in energetic regions. However, when applied to the study of Gulf Stream rings, these products have formation patterns, seasonality, and trends inconsistent with the Ring Census. We caution future users to validate whether an eddy identified by these SSH-based products is actually a Gulf Stream ring through use of temperature and salinity data, and, if possible, subsurface observations of the depth structure before making conclusions about Gulf Stream rings from an SSH eddy tracking product, such as META2.0, META3.1exp or GLED v1.0. More than SSH data is required to unequivocally identify Gulf Stream rings.

PEREZ ET AL. 18 of 22

## 5.3. Energy and Speed

In the analysis of satellite-derived surface geostrophic velocities in the Northwest Atlantic, a statistically significant regime shift in the EKE was detected in the year 2000 using the Rodionov change-point algorithm (*p*-value = 0.0013). The component that contributes most to the EKE in the Northwest Atlantic and seems to drive the shift to higher EKE after 2000 is concentrated in the Gulf Stream region and is associated with the Gulf Stream changing speed and position after 2000, particularly where the Gulf Stream interacts with the New England Seamount Chain (Figures 6 and 7). This shift to higher EKE in the entire system after 2000 coincides with the timing of the observed regime shift in WCRs. The year 2000 is also a pivotal point in the long-term SST trends in the Northwest Atlantic, as demonstrated by Chen et al. (2020).

Adjacent regions of increase and decrease in energy and speed near the mean position of the Gulf Stream may also point to a change in the Gulf Stream position, as a northward shift in the Gulf Stream has been observed in recent years (Gonçalves Neto et al., 2021; Todd & Ren, 2023). In fact, we find the area of the Slope Sea region decreased from 1993 to 2017, while the area of the Sargasso Sea region increased, indicating a northward shift of the Gulf Stream front (not shown). The energy and speed changes in the Gulf Stream sub-region and the Northwest Atlantic as a whole suggest that the increase in ring formations associated with the regime shift in 2000 is related to a more energetic, faster Gulf Stream. The implication is that a vigorously meandering Gulf Stream sheds more WCRs than a less energetic stream. The lack of increase in EKE in the Slope Sea after 2000 suggests that these rings may be reabsorbed by the meandering Gulf Stream relatively quickly so that they do not contribute to the EKE within the Slope Sea for a long duration.

The speed, KE, and EKE were computed from the same SSH data that the global eddy tracking products are based on, yet the global eddy products (unfiltered and filtered) do not capture the key characteristics of WCRs, such as seasonality, preferred formation location, and the observed regime shift in the year 2000. The authors of the various global eddy products acknowledge that the eddy tracker algorithms have difficulty identifying eddies in highly energetic western boundary current regions, such as the Gulf Stream. A shift to a higher EKE state in the Gulf Stream and the whole Northwest Atlantic region may further impede these algorithms' ability to identify mesoscale eddies in this region. Additionally, a recent paper from Martin et al. (2023) noted that gridded SSH products do not capture mesoscale variability in highly energetic currents such as the Gulf Stream because of the traditional method of interpolating between altimeter tracks. Martin et al. (2023) demonstrate that a deep learning model trained on altimetry and SST data reconstructs SSH fields with lower error and resolves smaller spatial scales than the traditional method of optimal interpolation. An eddy tracking algorithm input with higher resolution SSH fields may perform better than current algorithms since the smaller-scale variability is better resolved.

#### 6. Conclusions

The Ring Census is currently the longest record of WCRs publicly available and has been extensively validated, which is why it is used here as the standard against which the global altimetry-based eddy products are compared. Although both META products and GLED v1.0 fail to capture a regime shift in the formation of ring-like eddies, it is important to recognize the potential existence of such a shift, despite these products' failure to capture it. From the feature-by-feature analysis and the statistical comparisons, we know these products do not identify some of the key characteristics of WCRs (e.g., seasonality, preferred formation location, etc.). One drawback of using readily available SSH-based eddy tracking products to study Gulf Stream rings is that additional information, such as SST, sea surface salinity, or, ideally, subsurface hydrographic data, which could help confirm if eddies are indeed rings, is not used.

In summary, one difficulty in using global altimetry-based eddy products to study Gulf Stream rings is the limited spatial and temporal resolution of the SSH maps that these products rely on. Additionally, these products are designed to study mesoscale eddies, not necessarily ring-distinct features with temperature, salinity, and vertical signatures that the SSH eddy products cannot capture. Furthermore, the Gulf Stream, like all Western Boundary Currents, is a highly energetic region with many features on multiple space and time scales, which we do not consider rings but may be classified as eddies by these global SSH eddy products, further adding to the challenge of using those global products to study regional rings. A regional ring product (the Ring Census) does observe a regime shift in WCRs in 2000 and the global eddy products' failure to detect the regime shift in WCR-like eddies should not be interpreted as evidence against the regime shift.

PEREZ ET AL. 19 of 22



## Journal of Geophysical Research: Oceans

10.1029/2023JC020761

Notably, we find a regime shift in the EKE of the Northwest Atlantic at the year 2000 (p-value = 0.0013). This shift to a higher EKE state after 2000 is primarily driven by a synchronous shift in the EKE of the Gulf Stream. The increase in EKE is attributed to the change in the speed and position of the Gulf Stream after 2000. The implication is that a more energetic and meandering Gulf Stream sheds more rings.

Further understanding of (a) what is driving the regime shift and (b) why the global altimetry-based eddy products do not detect it will require further examination of the dynamics of the regime shift. New insights may also be gained with the new Surface Water Ocean Topography satellite altimeter (Wang et al., 2022), which will provide much improved spatial resolution of SSH maps. Ultimately, distinguishing rings and eddies requires sub-surface velocity and hydrographic data that is currently sparse in the world's oceans. Techniques that utilize only surface observations, even with improved horizontal resolution, will remain limited in their ability to unambiguously identify rings. Given the turbulent nature of the underlying flow field and the complexity of vertical gradients beneath the surface indicators, a high degree of uncertainty is expected.

## **Data Availability Statement**

The Warm Core Ring Census is available via https://www.bco-dmo.org/dataset/810182. The META2.0 and META3.1exp eddy data sets are available from AVISO+ at https://www.aviso.altimetry.fr/en/data/products/ value-added-products/global-mesoscale-eddy-trajectory-product/meta2-0-dt.html and https://www.aviso.altimetry.fr/en/data/products/value-added-products/global-mesoscale-eddy-trajectory-product/meta3-1-exp-dt.html, respectively. The altimetric Mesoscale Eddy Trajectories Atlas (META2.0) was produced by SSALTO/DUACS and distributed by AVISO+ (https://aviso.altimetry.fr) with support from CNES, in collaboration with Oregon State University with support from NASA. The altimetric Mesoscale Eddy Trajectories Atlas (META3.1exp DT) was produced by SSALTO/DUACS and distributed by AVISO+ with support from CNES, in collaboration with IMEDEA (https://doi.org/10.24400/527896/a01-2021.001 for the META3.1exp DT allsat version and https://doi. org/10.24400/527896/a01-2021.002 for the META3.1exp DT twosat version). The GLED v1.0 eddy data set is available from Zenodo at https://zenodo.org/record/7349753. The Regime Shift Detection software is available via https://sites.google.com/view/regime-shift-test/home. The 25 cm SSH contour identifies Gulf Stream daily paths. See Andres (2016) for more information on deriving Gulf Stream paths. Sea surface temperature (SST) data is available from https://www.ncei.noaa.gov/products/optimum-interpolation-sst. This study has been conducted using E.U. Copernicus Marine Service Information (2024): https://doi.org/10.48670/moi-00148. Monthly SSH data is available from https://data.marine.copernicus.eu/product/SEALEVEL GLO PHY L4 MY 008 047/ description. Gridded bathymetry data is available from https://www.gebco.net/data\_and\_products/gridded\_bathymetry\_data/. Code for analyzing and plotting the data is available upon reasonable request from the corresponding author.

The code used in the analyses described in this study is available in a GitHub repository: https://github.com/elenakperez/rings. The corresponding author can provide more information about the code upon a reasonable request.

## Acknowledgments References

E. Perez was supported by the NSF

Graduate Research Fellowship Program,

under Grants 2141064 and 1745302. M.

Andres was supported by NSF Project

OCE-2123111. G. Gawarkiewicz was

supported by NSF Project OCE-2122726.

The authors thank Avijit Gangopadhyay

anonymous reviewers greatly improved

the quality and presentation of this work;

the authors thank the reviewers for their

and Adrienne Silver for helpful

time and effort.

discussions. Comments from three

Abernathy, R., & Haller, G. (2018). Transport by Lagrangian vortices in the eastern Pacific. *Journal of Physical Oceanography*, 48(3), 667–685. https://doi.org/10.1175/JPO-D-17-0102.1

Andres, M. (2016). On the recent destabilization of the Gulf Stream path downstream of Cape Hatteras. *Geophysical Research Letters*, 43(18), 9836–9842. https://doi.org/10.1002/2016GL06996

Andres, M., Donohue, K. A., & Toole, J. M. (2020). The Gulf Stream's path and time-averaged velocity structure and transport at 68.5°W and 70.3°W. Deep Sea Research Part I: Oceanographic Research Papers, 156(103179), 103179. https://doi.org/10.1016/j.dsr.2019.103179

Bisagni, J. J., Kang, D., Thomas, A. C., & Schmidt, A. (2024). Surface eddy kinetic energy variability of the Western North Atlantic slope sea 1993–2016. Continental Shelf Research, 275, 105200. https://doi.org/10.1016/j.csr.2024.105200

Braun, C. D., Gaube, P., Sinclair-Taylor, T. H., Skomal, G. B., & Thorrold, S. R. (2019). Mesoscale eddies release pelagic sharks from thermal constraints to foraging in the ocean twilight zone. *Proceedings of the National Academy of Sciences of the United States of America*, 116(35), 17187–17192. https://doi.org/10.1073/pnas.1903067116

Brown, O. B., Cornillon, P. C., Emmerson, S. R., & Carle, H. (1986). Gulf Stream warm rings: A statistical study of their behavior. *Deep Sea Research Part A. Oceanographic Research Papers*, 33(11–12), 1459–1473. https://doi.org/10.1016/0198-0149(86)90062-2

Chelton, D. B., Schlax, M. G., & Samelson, R. M. (2011). Global observations of nonlinear mesoscale eddies. *Progress in Oceanography*, 91(2), 167–216. https://doi.org/10.1016/j.pocean.2011.01.002

Chelton, D. B., Schlax, M. G., Samelson, R. M., & de Szoeke, R. A. (2007). Global observations of large oceanic eddies. Geophysical Research Letters, 34, L15606. https://doi.org/10.1029/2007GL030812

Letters, 34, L15606. https://doi.org/10.1029/200/GL030812

PEREZ ET AL. 20 of 22

- Chen, Z., Kwon, Y. O., Chen, K., Fratantoni, P., Gawarkiewicz, G., & Joyce, T. M. (2020). Long-term SST variability on the Northwest Atlantic continental shelf and slope. *Geophysical Research Letters*, 47(1), e2019GL085455. https://doi.org/10.1029/2019GL085455
- Conway, T. M., Palter, J. B., & de Souza, G. F. (2018). Gulf Stream rings as a source of iron to the North Atlantic subtropical gyre. *Nature Geoscience*, 11(8), 594–598. https://doi.org/10.1038/s41561-018-0162-0
- Cornillon, P., Weyer, R., & Flierl, G. (1989). Translational velocity of warm core rings relative to the slope water. *Journal of Physical Oceanography*, 19(9), 1317–1332. https://doi.org/10.1175/1520-0485(1989)019\langle1317:TVOWCR\langle2.0.CO;2
- Csanady, G. T. (1979). The birth and death of a warm core ring. *Journal of Geophysical Research*, 84(C2), 777–780. https://doi.org/10.1029/ JC084iC02p00777
- E.U. Copernicus Marine Service Information. (2024). Global ocean gridded L4 sea surface heights and derived variables reprocessed 1993 ongoing. Marine Data Store (MDS). https://doi.org/10.48670/moi-00148
- Faghmous, J. H., Frenger, I., Yao, Y., Warmka, R., Lindell, A., & Kumar, V. (2015). A daily global mesoscale ocean eddy dataset from satellite altimetry. *Nature Scientific Data*, 2, 150028. https://doi.org/10.1038/sdata.2015.28
- Flierl, G. R. (1979). A simple model for the structure of warm and cold core rings. *Journal of Geophysical Research*, 84(C2), 781–785. https://doi.org/10.1029/JC084iC02p00781
- Forsyth, J. S. T., Andres, M., & Gawarkiewicz, G. G. (2015). Recent accelerated warming of the continental shelf off New Jersey: Observations from the CMV oleander expendable bathythermograph line. *Journal of Geophysical Research: Oceans*, 120(3), 2370–2384. https://doi.org/10.1002/2014JC010516
- Fuglister, F. C. (1972). Cyclonic rings formed by the Gulf Stream 1965-66. Studies in Physical Oceanography, 137–168. Retrieved from https://cir.nii.ac.jp/crid/1573950399590787712
- Gangopadhyay, A., & Gawarkiewicz, G. (2020). Yearly census of Gulf Stream warm core ring formation from 1980 to 2017. (version 1) version date 2020-05-06 [Dataset]. Biological and Chemical Oceanography Data Management Office (BCO-DMO). Retrieved from https://www.bco-dmo.org/dataset/810182
- Gangopadhyay, A., Gawarkiewicz, G., Silva, E. N. S., Monim, M., & Clark, J. (2019). An observed regime shift in the formation of warm core rings from the Gulf Stream. Scientific Reports, 9(1), 12319. https://doi.org/10.1038/s41598-019-48661-9
- Gangopadhyay, A., Gawarkiewicz, G., Silva, E. N. S., Silver, A. M., Monim, M., & Clark, J. (2020). A census of the warm-core rings of the Gulf Stream: 1980–2017. *Journal of Geophysical Research: Oceans*, 125(8), e2019JC016033. https://doi.org/10.1029/2019JC016033
- Gawarkiewicz, G., Fratantoni, P., Bahr, F., & Ellertson, A. (2022). Increasing frequency of mid-depth salinity maximum intrusions in the middle Atlantic bight. *Journal of Geophysical Research: Oceans*, 127(7), e2021JC018233. https://doi.org/10.1029/2021JC018233
- Gawarkiewicz, G., Todd, R., Zhang, W., Partida, J., Gangopadhyay, A., Monim, M. U. H., et al. (2018). The changing nature of shelf-break exchange revealed by the OOI Pioneer Array. *Oceanography*, 31(1), 60–70. https://doi.org/10.5670/oceanog.2018.110
- Gonçalves Neto, A., Langan, J. A., & Palter, J. B. (2021). Changes in the Gulf Stream preceded rapid warming of the Northwest Atlantic shelf.
- Nature Communications Earth and Environment, 2(74), 74. https://doi.org/10.1038/s43247-021-00143-5
  Haller, G., Hadjighasem, A., Farazmand, M., & Huhn, F. (2016). Defining coherent vortices objectively from the vorticity. Journal of Fluid
- Mechanics, 795, 136–173. https://doi.org/10.1017/jfm.2016.151
  Hamilton, P., Fargion, G. S., & Biggs, D. C. (1999). Loop current eddy paths in the western Gulf of Mexico. Journal of Physical Oceanography,
- 29(6), 1180–1207. https://doi.org/10.1175/1520-0485(1999)029(1180:LCEPIT)2.0.CO:2

  Holliday, N. P., Bersch, M., Berx, B., Chafik, L., Cunningham, S., Florindo-López, C., et al. (2020). Ocean circulation causes the largest
- freshening event for 120 years in eastern subpolar North Atlantic. *Nature Communications*, 11(585), 585. https://doi.org/10.1038/s41467-020-14474-y
- Huang, B., Liu, C., Banzon, V., Freeman, E., Graham, G., Hankins, B., et al. (2020). Improvements of the daily optimum interpolation sea surface temperature (DOISST) version 2.1. *Journal of Climate*, 34(8), 2923–2939. https://doi.org/10.1175/JCLI-D-20-0166.1
- Isern-Fontanet, J., Font, J., García-Ladona, E., Emelianov, M., Millot, C., & Taupier-Letage, I. (2004). Spatial structure of anticyclonic eddies in the Algerian basin (Mediterranean Sea) analyzed using the Okubo–Weiss parameter. *Deep-Sea Research*, 31, L24311. https://doi.org/10.1016/j.dsr2.2004.09.013
- Isern-Fontanet, J., García-Ladona, E., & Font, J. (2003). Identification of marine eddies from altimetric maps. *Journal of Atmospheric and Oceanic Technology*, 20(5), 772–778. https://doi.org/10.1175/1520-0426(2003)20(772:IOMEFA)2.0.CO;2
- Joyce, T. M. (1984). Velocity and hydrographic structure of a Gulf Stream warm-core ring. Journal of Geophysical Research, 14(5), 936–947. https://doi.org/10.1175/1520-0485(1984)014(0936;VAHSOA)2.0.CO;2
- Joyce, T. M. (1991). Review of U. S. contributions to warm-core rings. Reviews of Geophysics, 29(S2), 610–616. https://doi.org/10.1002/rog. 1991.29.s2.610
- Kang, D., Curchitser, E. N., & Rosati, A. (2016). Seasonal variability of the Gulf Stream kinetic energy. *Journal of Physical Oceanography*, 46(4), 1189–1207. https://doi.org/10.1175/JPO-D-15-0235.1
- Kurian, J., Colas, F., Capet, X., McWilliams, J. C., & Chelton, D. B. (2011). Eddy properties in the California current system. *Journal of Geophysical Research*, 116, C08027. https://doi.org/10.1029/2010JC006895
- Lambhate, D., Sharma, R., Clark, J., Gangopadhyay, A., & Subramani, D. (2021). W-Net: A deep network for simultaneous identification of gulf stream and rings from concurrent satellite images of sea surface temperature and height. IEEE Transactions on Geoscience and Remote Sensing, 60(4203213), 1–13. https://doi.org/10.1109/TGRS.2021.3096202
- Liu, T., & Abernathey, R. (2022). A global Lagrangian eddy dataset based on satellite altimetry (gled v1.0) (v1.0) [Dataset]. Zenodo. https://doi.org/10.5281/zenodo.7349753
- Liu, T., & Abernathey, R. (2023). A global Lagrangian eddy dataset based on satellite altimetry. Earth System Science Data, 15(4), 1765–1778. https://doi.org/10.5194/essd-15-1765-2023
- Lutjeharms, J. R. E. (1981). Features of the southern Agulhas Current circulation from satellite remote sensing. South African Journal of Science, 77(5), 231–236. https://doi.org/10.10520/AJA00382353\_1526
- Martin, S. A., Manucharyan, G. E., & Klein, P. (2023). Synthesizing sea surface temperature and satellite altimetry observations using deep learning improves the accuracy and resolution of gridded sea surface height anomalies. *Journal of Advances in Modeling Earth Systems*, 15(5), e2022MS003589. https://doi.org/10.1029/2022MS003589
- Mason, E., Pascual, A., & McWilliams, J. C. (2014). A new sea surface height-based code for oceanic mesoscale eddy tracking. *Journal of Atmospheric and Oceanic Technology*, 31(5), 1181–1188. https://doi.org/10.1175/JTECH-D-14-00019.1
- Monim, M. (2017). Seasonal and inter-annual variability of Gulf Stream warm core rings from 2000 to 2016 (p. 113). MS Thesis, University of Massachusetts Dartmouth.
- Morrow, R., Birol, F., Griffin, D., & Sudre, J. (2004). Divergent pathways of cyclonic and anti-cyclonic ocean eddies. Geophysical Research Letters, 31, L24311. https://doi.org/10.1029/2004GL020974

PEREZ ET AL. 21 of 22

- Nencioli, F., Dong, C., Dickey, T., Washburn, L., & McWilliams, J. C. (2010). A vector geometry-based eddy detection algorithm and its application to a high-resolution numerical model product and high-frequency radar surface velocities in the southern California bight. *Journal* of Atmospheric and Oceanic Technology, 27(3), 564–579. https://doi.org/10.1175/2009JTECHO725.1
- Pegliasco, C., Delepoulle, A., Mason, E., Morrow, R., Faugère, Y., & Dibarboure, G. (2022). Meta3.1exp: A new global mesoscale eddy trajectory atlas derived from altimetry. Earth System Science Data, 14(3), 1087–1107. https://doi.org/10.5194/essd-14-1087-2022
- Pershing, A. J., Alexander, M. A., Hernandez, C. M., Kerr, L. A., Le Bris, A., Mills, K. E., et al. (2015). Slow adaptation in the face of rapid warming leads to collapse of the Gulf of Maine cod fishery. *Science*, 350(6262), 809–812. https://doi.org/10.1126/science.aac9819
- Richardson, A. R. (1983). Eddies in marine science. Springer.
- Richardson, P. L., Cheney, R. E., & Worthington, L. V. (1978). A census of Gulf Stream rings. Studies in Physical Oceanography, 83(C12), 6136–6144. https://doi.org/10.1029/jc083ic12p06136
- Rodionov, S. N. (2004). A sequential algorithm for testing climate regime shifts. Geophysical Research Letters, 31(9), L09204. https://doi.org/10.1029/2004GL019448
- Schlax, M. G., & Chelton, D. B. (2016). The "growing method" of eddy identification and tracking in two and three dimensions. College of Earth, Ocean and Atmospheric, Oregon State University Sciences. Retrieved from https://www.aviso.altimetry.fr/fileadmin/documents/data/products/value-added/Schlax\_Chelton\_2016.pdf
- Shadden, S. C., Lekien, F., & Marsden, J. E. (2005). Definition and properties of Lagrangian coherent structures from finite-time Lyapunov exponents in two-dimensional aperiodic flows. *Physica D: Nonlinear Phenomena*, 212(3–4), 271–304. https://doi.org/10.1016/j.physd.2005. 10.007
- Silva, E. N. S. (2019). Understanding thirty-eight years of Gulf Stream's warm core rings: Variability, regimes and survival (p. 125). MS Thesis. University of Massachusetts Dartmouth.
- Silver, A., Gangopadhyay, A., Gawarkiewicz, G., Andres, M., Flierl, G., & Clark, J. (2022). Spatial variability of movement, structure, and formation of warm core rings in the northwest Atlantic Slope Sea. *Journal of Geophysical Research: Oceans*, 127(8), e2022JC018737. https://doi.org/10.1029/2022JC018737
- Silver, A., Gangopadhyay, A., Gawarkiewicz, G., Fratantoni, P., & Clark, J. (2023). Increased Gulf Stream warm core ring formations contributes to an observed increase in salinity maximum intrusions on the northeast shelf. *Scientific Reports*, 13(7538), 7538. https://doi.org/10.1038/s41598-023-34494-0
- Silver, A., Gangopadhyay, A., Gawarkiewicz, G., Silva, E. N. S., & Clark, J. (2021). Interannual and seasonal asymmetries in Gulf Stream ring formations from 1980 to 2019. Scientific Reports, 11(1), 2207. https://doi.org/10.1038/s41598-021-81827-y
- Todd, R. E., & Ren, A. S. (2023). Warming and lateral shift of the Gulf Stream from in situ observations since 2001. *Nature Climate Change*, 13(12), 1348–1352. https://doi.org/10.1038/s41558-023-01835-w
- Wang, J., Fu, L. L., Haines, B., Lankhorst, M., Lucas, A. J., Farrar, J. T., et al. (2022). On the development of swot in situ calibration/validation for short-wavelength ocean topography. *Journal of Atmospheric and Oceanic Technology*, 39(5), 595–617. https://doi.org/10.1175/JTECH-D-21-0039 1
- Zhai, X., Greatbatch, R. J., & Kohlmann, J. D. (2008). On the seasonal variability of eddy kinetic energy in the Gulf Stream region. *Geophysical Research Letters*, 35(24), L24609. https://doi.org/10.1029/2008GL036412
- Zhang, W. G., & Gawarkiewicz, G. G. (2015). Dynamics of the direct intrusion of gulf stream ring water onto the mid-Atlantic bight shelf. Geophysical Research Letters, 42(18), 7687–7695. https://doi.org/10.1002/2015GL065530

PEREZ ET AL. 22 of 22